EQUATION OF STATE AND OPACITIES FOR HYDROGEN ATMOSPHERES OF NEUTRON STARS WITH STRONG MAGNETIC FIELDS

Alexander Y. Potekhin

Ioffe Physico-Technical Institute, Politekhnicheskaya 26, 194021 St. Petersburg, Russia; and Isaac Newton Institute of Chile,
St. Petersburg Branch, Russia; palex@astro.ioffe.rssi.ru

and

Gilles Chabrier

Ecole Normale Supérieure de Lyon (CRAL, UMR CNRS 5574), 46 Allée d'Italie, 69364 Lyon Cedex 07, France; chabrier@ens-lyon.fr

ABSTRACT

We present an equation of state and radiative opacities for a strongly magnetized hydrogen plasma at magnetic fields B, temperatures T, and densities ρ typical for atmospheres of isolated neutron stars. The first- and second-order thermodynamic functions, monochromatic radiative opacities, and Rosseland mean opacities are calculated and tabulated, taking account of partial ionization, for 8×10^{11} G $\leq B \leq 3 \times 10^{13}$ G, 2×10^5 K $\leq T \leq 10^7$ K, and a wide range of ρ. We show that bound-bound and bound-free transitions give an important contribution to the opacities at $T \lesssim (1–5) \times 10^6$ K in the considered range of B in the outer neutron star atmosphere layers, which may substantially modify the X-ray spectrum of a typical magnetized neutron star. In addition, we reevaluate opacities due to free-free transitions, taking into account the motion of both interacting particles, electron and proton, in a strong magnetic field. Compared to the previous neutron star atmosphere models, the free-free absorption is strongly suppressed at photon frequencies below the proton cyclotron frequency. The latter result holds for any field strength, which prompts a revision of existing theoretical models of X-ray spectra of magnetar atmospheres.

Subject headings: equation of state — magnetic fields — plasmas — stars: atmospheres — stars: neutron

1. INTRODUCTION

Models of neutron star atmospheres are needed for interpretation of their spectra and cooling. These atmospheres differ from the atmospheres of ordinary stars because of the high gravity and magnetic fields (for review see, e.g., Pavlov et al. 1995; Ventura & Potekhin 2001).

A magnetic field is called *strong* if the electron cyclotron energy $\hbar\omega_{ce} = \hbar eB/m_e c$ exceeds 1 a.u.; i.e., the field strength B is higher than $B_0 = m_e^2 c e^3/\hbar^3 = 2.3505 \times 10^9$ G, where m_e is the electron mass, e the elementary charge, and c the speed of light. Usually the field is called *superstrong* if $\hbar\omega_{ce} > m_e c^2$, that is, $B > B_r = m_e^2 c^3/e\hbar = 4.414 \times 10^{13}$ G. Most of the radio pulsars have magnetic fields $B \sim 10^{12}$–10^{13} G (Taylor, Manchester, & Lyne 1993), whereas anomalous X-ray pulsars and soft gamma repeaters are thought to have superstrong fields (e.g., Mereghetti 2001; Thompson et al. 2000 and references therein). Nonnegligible amounts of neutral atoms can exist in the photosphere at typical neutron star temperatures $T \sim 10^6$ K (Potekhin, Chabrier, & Shibanov 1999, hereafter Paper I). A strong magnetic field enhances atomic binding and makes the quantum mechanical characteristics of an atom dependent on its motion across the field (for a recent review see Lai 2001). In photospheres of the neutron stars, the field is, as a rule, *strongly quantizing*; i.e., it sets all the electrons on the ground Landau level. This occurs if $\beta_e \gg 1$ and $\rho < \rho_B$, where

$$\beta_e = \frac{\hbar\omega_{ce}}{k_B T} \approx 134.3 \frac{B_{12}}{T_6} \ , \qquad (1)$$

ρ is the density, and $\rho_B = m_H/(\pi^2\sqrt{2}a_m^3) \approx 7100 B_{12}^{3/2}$ g cm^{-3} (for the hydrogen plasma). Here and hereafter,

$m_H = m_p + m_e$, m_p is the proton mass, $a_m = (\hbar c/eB)^{1/2}$ is the *magnetic length*, k_B is the Boltzmann constant, $B_{12} = B/10^{12}$ G, and $T_6 = T/10^6$ K.

Opacities for the two polarization modes of radiation are quite different in strongly magnetized plasmas (e.g., Pavlov et al. 1995 and references therein), which makes thermal emission of neutron stars polarized and anisotropic (Zavlin et al. 1995). The mean opacities are strongly reduced at $\beta_e \gg 1$ (e.g., Silant'ev & Yakovlev 1980); thus, the bottom of the photosphere is shifted to high densities (e.g., Pavlov et al. 1995; Lai & Salpeter 1997).

The chemical composition of neutron star atmospheres is not precisely known. Just after the neutron star birth in a supernova explosion, the outer stellar envelope is most probably composed of iron. However, light elements may be brought to the surface later (e.g., by fallback, accretion, or encounters with comets). Because of rapid gravitational sedimentation, the lightest element will cover the surface (see Brown, Bildsten, & Chang 2002). About 10^{12}–10^{14} g of hydrogen ($<10^{-19}\ M_\odot$) is sufficient to fill the entire photosphere.

Shibanov et al. (1992) presented the first model of hydrogen atmospheres with strong magnetic fields. Later it was developed beyond the diffusion approximation (Shibanov & Zavlin 1995) and used for astrophysical predictions (e.g., Zavlin et al. 1995; Zane, Turolla, & Trevis 2000; Zane et al. 2001; Ho & Lai 2001, 2003; Lai & Ho 2002; Özel 2001, 2003) and for interpretation of observed neutron star spectra (e.g., Page, Shibanov, & Zavlin 1995, 1996; Pavlov et al. 1995; Özel, Psaltis, & Kaspi 2001).

The above studies assume that the atmosphere is fully ionized. Meanwhile, it was recognized long ago (e.g., Miller 1992) that a significant contribution to the opacities of

neutron star photospheres with strong magnetic fields might come from bound-bound and bound-free absorption by atoms. Examples of monochromatic opacities in partially ionized iron (Rajagopal, Romani, & Miller 1997) and hydrogen (Potekhin, Chabrier, & Shibanov 2000) atmospheres confirmed this conjecture. In Paper I we have presented an equation of state (EOS) of a partially ionized hydrogen plasma for the values of T and B typical for atmospheres of the radio pulsars. Here we report results of extensive calculations of thermodynamic functions based on the theory developed in Paper I, supplemented by calculations of the opacities (monochromatic and Rosseland mean). Partial ionization and plasma nonideality are taken into account for $11.9 \leq \log_{10} B/\mathrm{G} \leq 13.5$ and $5.3 \leq \log_{10} T/\mathrm{K} \leq 7.0$. Bound-bound and bound-free radiative transitions are treated within the framework of a previously developed theory (Pavlov & Potekhin 1995; Potekhin & Pavlov 1997). The free-free absorption cross sections are reevaluated. Whereas the previous authors considered photoabsorption by an electron scattered off a fixed Coulomb center, we take into account the finite proton mass, which has a nontrivial effect on the photoabsorption in a quantizing magnetic field.

The paper is composed as follows. In § 2 we formulate the main assumptions and give the basic formulae used in our work. In § 3 we present the EOS of partially ionized hydrogen under conditions in neutron star photospheres. In § 4 we discuss various contributions to the hydrogen photoabsorption cross sections in strong magnetic fields and derive a new formula for the free-free cross section. Opacities of hydrogen photospheres of the neutron stars are discussed in § 5. Appendices give some detail of calculation of the free-free cross sections.

2. BASIC EQUATIONS AND PHYSICS INPUT

2.1. *Hydrogen Atom Moving in a Magnetic Field*

If an atom rests without motion in a strong magnetic field, there are two distinct classes of its quantum states: at every value of the Landau quantum number n and the magnetic quantum number $-s$ ($n \geq 0$, $s \geq -n$), there is one tightly bound state, with binding energy growing asymptotically as $[\ln(B/B_0)]^2$, and an infinite series of hydrogen-like states with binding energies approaching the energies of a field-free H atom (e.g., Canuto & Ventura 1977). The atom is elongated: its size along the magnetic field B either decreases logarithmically (for the tightly bound states) or remains nearly constant (for the hydrogen-like states), while the transverse radius is close to a_m, decreasing as $B^{-1/2}$. The radiative transition rates are different for the three basic polarizations: the linear polarization along the field and the two circular polarizations in the transverse plane.

This simplicity is destroyed when atomic motion is taken into account. The electric field, induced in the comoving frame of reference, breaks down the cylindrical symmetry. In the nonrelativistic quantum mechanics, the binding energies and wave functions of the H atom are given by a solution of the Schrödinger equation with the two-particle Hamiltonian

$$H = \frac{\pi_e^2}{2m_p} + \frac{\pi_e^2}{2m_e} - \frac{e^2}{|r_e - r_p|} \, , \qquad (2)$$

where m_i, r_i, and π_i are the mass, radius, and kinetic momentum of the electron ($i = e$) or proton ($i = p$). The kinetic momentum (related to the velocity) equals (e.g., Landau & Lifshitz 1976)

$$\pi_i = p_i - \frac{q_i}{c} A(r_i) \, , \qquad (3)$$

where q_i is the charge of the ith particle ($q_e = -q_p = -e$), p_i is the canonical momentum (i.e., $p_i = -i\hbar\nabla_i$ in the coordinate representation), and $A(r)$ is the vector potential of the field. A conserved quantity related to the center-of-mass motion is the *pseudomomentum*

$$K = \pi_p + \pi_e + \frac{e}{c} B \times (r_p - r_e) \, . \qquad (4)$$

Let the z-axis of the Cartesian coordinates (x, y, z) be directed along B. Separating the center-of-mass motion (Gor'kov & Dzyaloshinskii 1967; Vincke, Le Dourneuf, & Baye 1992; Potekhin 1994) and choosing the gauge of the vector potential in the form

$$A(r) = \frac{1}{2} B \times \left(r - \frac{m_p - m_e}{m_\mathrm{H}} r_0 \right) \, , \qquad (5)$$

where r_0 is arbitrary, one comes to the effective one-particle Schrödinger equation

$$\left(\frac{p_z^2}{2\mu} + H_\perp + H_K(r_0) - \frac{e^2}{|r_0 + r|} \right) \psi(r) = E\psi(r) \, . \qquad (6)$$

Here $r = r_e - r_p - r_0$ is a "shifted" relative coordinate, $p_z = -i\hbar\partial/\partial z$ is the z-component of its conjugate momentum p,

$$H_\perp = \frac{\pi_\perp^2}{2\mu} - \frac{e}{m_p c} B \cdot (r \times p) \, , \qquad (7)$$

$$H_K(r_0) = \frac{1}{2m_\mathrm{H}} \left(K + \frac{e}{c} B \times r_0 \right)^2 + \frac{e}{m_\mathrm{H} c} \left(K + \frac{e}{c} B \times r_0 \right) \cdot (B \times r) \, , \qquad (8)$$

and $\mu = m_e m_p / m_\mathrm{H}$ is the reduced mass. In equation (7),

$$\pi = p + \frac{e}{2c} B \times r \qquad (9)$$

and the subscript "$\perp$" denotes a vector component perpendicular to B.

$H_K(r_0)$ turns to zero, if we set $r_0 = r_c$, where

$$r_c = \frac{c}{eB^2} B \times K \qquad (10)$$

is the relative guiding center (the difference between the electron and proton guiding centers). This choice of r_0 is most useful for bound states with large $K_\perp$ and the states of the continuum, whereas for bound states with small $K_\perp$ the choice $r_0 = 0$ is most appropriate (Potekhin 1994; Potekhin & Pavlov 1997).

The eigenfunctions of $H_\perp$ are the Landau functions $\Phi_{ns}(r_\perp)$ (given, e.g., by eq. [5] of Potekhin & Pavlov 1993), with eigenenergies

$$E_{ns}^\perp = n\hbar\omega_\mathrm{ce} + (n + s)\hbar\omega_\mathrm{cp} \, , \qquad (11)$$

where $\omega_\mathrm{cp} = (m_e/m_p)\omega_\mathrm{ce}$ is the proton cyclotron frequency.

It is convenient to expand the wave function on the basis of $\Phi_{ns}(\mathbf{r}_\perp)$,

$$\psi(\mathbf{r}) = \sum_{n's'} g_{n's'}(z)\Phi_{n's'}(\mathbf{r}_\perp) \,, \qquad (12)$$

and to label $\psi(\mathbf{r})$ by numbers n and s, corresponding to the leading term of this expansion. The third quantum number ν then enumerates "longitudinal" energy levels. The *adiabatic approximation* widely used in the past (e.g., Gor'kov & Dzyaloshinskii 1967; Canuto & Ventura 1977) corresponds to retaining only one term $n' = n$, $s' = s$ in equation (12). We perform calculations without this approximation.

The total energy of the atom in equation (6) can be written as

$$E = E_{ns}^\perp + E_{ns\nu}^\parallel(K_\perp) \,. \qquad (13)$$

Here the *longitudinal energy* $E_{ns\nu}^\parallel(K_\perp)$ is negative for the bound and autoionizing (resonance) states and positive for the continuum states, in which the motion along z is infinite (in the latter case, ν is continuous). Since $n = 0$ for the bound states of an H atom in a strong magnetic field, we will drop the number n but imply $n = 0$ for these states. Then the binding energy is

$$\epsilon_{s\nu}(K_\perp) = \left| E_{s\nu}^\parallel(K_\perp) \right| - s\hbar\omega_{\rm cp} \,. \qquad (14)$$

The substitution of equation (12) in equation (6) reduces the problem to the set of the *coupled channel equations*

$$\left(\frac{p_z^2}{2\mu} + E_{n's'}^\perp - E \right) g_{n's'}(z) + \sum_{n'',s''} V_{n''s'',n's'}^{\rm tot}(z) g_{n's''}(z) = 0 \,, \qquad (15)$$

where

$$V_{ns,n's'}^{\rm tot}(z) = \langle ns|H_K(\mathbf{r}_0)|n's'\rangle_\perp + V_{ns,n's'}(\mathbf{r}_0, z) \qquad (16)$$

is a total coupling potential and

$$V_{ns,n's'}(\mathbf{r}_0, z) = \left\langle ns \left| \frac{-e^2}{|\mathbf{r}_0 + \mathbf{r}|} \right| n's' \right\rangle_\perp \qquad (17)$$

is an effective Coulomb potential. Here

$$\langle ns|f(\mathbf{r})|n's'\rangle_\perp = \int \Phi_{ns}^*(\mathbf{r}_\perp)f(\mathbf{r})\Phi_{n's'}(\mathbf{r}_\perp)d^2\mathbf{r}_\perp \,. \qquad (18)$$

Numerical solutions of equation (6) for various $K_\perp$ were presented by Vincke et al. (1992). At superstrong fields, binding energies were calculated by Lai & Salpeter (1995). The system of equations given by equation (15) was numerically solved for the discrete atomic states by Potekhin (1994) and for the continuum by Potekhin & Pavlov (1997). According to these studies, an atom moving across the strong magnetic field acquires a constant dipole moment parallel to $\mathbf{r}_c$. Those radiative transitions, which were dipole forbidden for an atom at rest because of conservation of the z-projection of the angular momentum, become allowed and should be taken into account in the atmosphere models. If $K_\perp$ is small enough, the dipole moment is also small. When $K_\perp$ exceeds a certain critical value, the atom becomes *decentered*: the average distance between the electron and proton approaches r_c. In this case, $K_\perp$ characterizes the electron-proton distance, rather than the atomic velocity. The binding energies (eq. [14]) decrease with increasing $K_\perp$. Asymptotically, at large $K_\perp$, all longitudinal energies tend

to $-e^2/r_c$. In this limit, the cylindrical symmetry of the wave function and dipole selection rules are restored, but the axis of symmetry is shifted to the distance r_c from the Coulomb center.

2.2. *Thermodynamic Model*

The EOS for partially ionized hydrogen in strong magnetic fields was constructed and discussed in Paper I. We employ the free-energy minimization technique in the "chemical picture" of a plasma (for discussion of its advantages and limitations see, e.g., Saumon, Chabrier, & Van Horn 1995; Potekhin 1996b). The treatment is based on the framework of the free-energy model developed by Saumon & Chabrier (1991, 1992) at $B = 0$ (see also Saumon et al. 1995 and § 2 of Paper I) and extends it to the strong magnetic field case.

We consider a plasma composed of N_p protons, N_e electrons, $N_{\rm H}$ hydrogen atoms, and $N_{\rm mol}$ molecules in a volume V, the number densities being $n_j \equiv N_j/V$. The Helmholtz free energy is written as the sum

$$F = F_{\rm id}^e + F_{\rm id}^p + F_{\rm id}^{\rm neu} + F_{\rm ex}^{\rm C} + F_{\rm ex}^{\rm neu} \,, \qquad (19)$$

where $F_{\rm id}^e$, $F_{\rm id}^p$, and $F_{\rm id}^{\rm neu}$ are the free energies of ideal gases of the electrons, protons, and neutral species, respectively, $F_{\rm ex}^{\rm C}$ takes into account the Coulomb plasma nonideality, and $F_{\rm ex}^{\rm neu}$ is the nonideal contribution that arises from interactions of bound species with each other and with the electrons and protons. In equation (19) we have disregarded the additive contribution due to photons, since it does not affect ionization equilibrium. Moreover, generally we need not assume thermodynamic equilibrium of radiation with matter. Ionization equilibrium is given by minimization of F with respect to particle numbers under the stoichiometric constraints, provided that the total number N_0 of protons (free and bound) is fixed. The latter number is determined by the total mass density: $n_0 \equiv N_0/V \approx \rho/m_{\rm H}$.

The first term in equation (19) is $F_{\rm id}^e = \mu_e N_e - P_e V$, where μ_e and P_e are the chemical potential and pressure of the ideal Fermi gas, respectively. They are obtained as functions of the electron number density n_e and temperature T from equations (e.g., Blandford & Hernquist 1982)

$$P_e = P_r \frac{b\tau_0^{3/2}}{\sqrt{2}\pi^2} \sum_{n=0}^\infty (2 - \delta_{n0})(1 + 2bn)^{1/4} I_{1/2}(\chi_n, \tau_n) \,, \qquad (20)$$

$$n_e = \lambda_{\rm C}^{-3} \frac{\tau_0 b}{2\pi^2} \sum_{n=0}^\infty (2 - \delta_{n0}) \left[\sqrt{\frac{2}{\tau_n}} \frac{\partial}{\partial \chi_n} I_{1/2}(\chi_n, \tau_n) \right] \,, \qquad (21)$$

where

$$I_{1/2}(\chi, \tau) = \int_0^\infty (e^{t-\chi} + 1)^{-1} \sqrt{t\left(1 + \frac{\tau t}{2}\right)} dt \,,$$

$$\chi_n = \frac{\mu_e}{k_B T} + \tau_0^{-1} - \tau_n^{-1}, \quad \tau_n = \frac{T/T_{\rm r}}{\sqrt{1 + 2bn}} \,,$$

and $b = (B/B_r)$. In these equations, $\lambda_{\rm C} = \hbar/(m_e c)^2 \approx 3.8616 \times 10^{-11}$ cm, $P_r = m_e c^2/\lambda_{\rm C}^3 \approx 1.4218 \times 10^{25}$ dyn cm^{-2}, and $T_r = m_e c^2/k_{\rm B} \approx 5.930 \times 10^9$ K are the relativistic units of length, pressure, and temperature, respectively, and $m_e c^2$ is *not* included in μ_e. We employ analytic fitting formulae to the standard Fermi-Dirac integral $I_{1/2}$ in equation (20) and to the expression in square brackets in equation

(21), accurate within a few parts in 10^3. These fits are presented, respectively, in § 3 of Chabrier & Potekhin (1998) and in Appendix C of Potekhin (1996a). When the electrons are nonrelativistic (as usually in the photospheres), equations (20) and (21) reproduce equations (30) and (31) of Paper I.

The Coulomb free-energy contribution consists of three parts, $F_{\mathrm{ex}}^{\mathrm{C}} = F_{pp} + F_{ee} + F_{pe}$, which represent, respectively, the proton-proton, electron-electron, and proton-electron interactions. There was no detailed study of the influence of a strong magnetic field on these contributions in the ρ and T domain we are interested in. Therefore, we employ nonmagnetic expressions (Chabrier & Potekhin 1998; Potekhin & Chabrier 2000), scaled with B. Specifically, the nonmagnetic expression for F_{pe} is based on numerical results obtained in the hypernetted chain approximation for the linear response theory with a local field correction (Chabrier 1990). The nonmagnetic expressions for F_{pp} and F_{ee} result from fitting the most accurate numerical results available in the literature (see Potekhin & Chabrier 2000 for references). In the strong magnetic field, the B-scaling of the nonmagnetic $F_{\mathrm{ex}}^{\mathrm{C}}$ is constructed so as to match known low- and high-density limits (§ IIIB of Paper I).

The free energy of nondegenerate and nonrelativistic gas of protons, F_{id}^{p}, is given by

$$\frac{F_{\mathrm{id}}^{p}}{N_p k_{\mathrm{B}} T} = \ln\left(2\pi a_m^2 \lambda_p n_p\right) + \ln\left(1 - e^{-\beta_p}\right) - 1$$
$$+ \frac{\beta_p}{2} - \ln\left[2\cosh\left(\frac{g_p \beta_p}{4}\right)\right], \quad (22)$$

where $g_p = 5.585$ is the proton gyromagnetic factor, $\lambda_p = \hbar[2\pi/(k_{\mathrm{B}} T m_p)]^{1/2}$ is the proton thermal wavelength, and $\beta_p = \hbar\omega_{\mathrm{cp}}/k_{\mathrm{B}} T \approx 0.0732 B_{12}/T_6$.

Let $N_{s\nu}$ be the total number of H atoms with given quantum numbers s and ν in the volume V, and let $p_{s\nu}(K_\perp)d^2K_\perp$ be the probability for such an atom to have a transverse pseudomomentum in an element $d^2K_\perp$ around $K_\perp$. Then the ideal part of the free energy for hydrogen atoms is

$$F_{\mathrm{id}}^{\mathrm{H}} = k_{\mathrm{B}} T \sum_{s\nu} N_{s\nu} \int \left\{ \ln\left[N_{s\nu} \lambda_{\mathrm{H}} \frac{(2\pi\hbar)^2}{V} p_{s\nu}(K_\perp) \right] \right.$$
$$\left. - 1 - \frac{\epsilon_{s\nu}(K_\perp)}{k_{\mathrm{B}} T} \right\} p_{s\nu}(K_\perp) d^2K_\perp$$
$$+ N_{\mathrm{H}} k_{\mathrm{B}} T \left\{ \frac{\beta_p}{2} - \ln\left[2\cosh\left(\frac{g_p \beta_p}{4}\right)\right] \right\}, \quad (23)$$

where $\lambda_{\mathrm{H}} \approx \lambda_p$ is the thermal wavelength of an atom. The probability density $p_{s\nu}(K_\perp)$ is calculated in a thermodynamically consistent way from derivatives of the *total* free energy F with respect to the particle numbers. Molecules H_2 are treated in an approximate manner, without taking into account their excited states and possible effects caused by their motion across the magnetic field and rotation. Finally, the nonideal part of the free energy of neutral species, $F_{\mathrm{ex}}^{\mathrm{neu}}$, is obtained in frames of the hard-sphere model, with effective radii depending on the quantum numbers *and pseudomomenta* of interacting atoms (see Paper I for detail).

Once the free energy is obtained, its derivatives over ρ and T and their combinations provide the other thermodynamic functions.

2.3. *Polarization Modes and Opacities: Basic Relations*

Propagation of radiation in magnetized plasmas was discussed in many papers and monographs (e.g., Ginzburg 1970). At photon energies $\hbar\omega$ much higher than

$$\hbar\omega_{\mathrm{pl}} = \left(\frac{4\pi\hbar^2 e^2 n_e}{m_e}\right)^{1/2} \approx 28.7\rho_0^{1/2} \ \mathrm{eV}, \quad (24)$$

where ω_{pl} is the electron plasma frequency and $\rho_0 \equiv \rho/(\mathrm{g\ cm^{-3}})$, radiation propagates in the form of *extra-ordinary* (hereafter labeled by index $j = 1$) and *ordinary* ($j = 2$) normal modes. These modes have different polarization vectors e_j and different absorption and scattering coefficients, which depend on the angle θ_B between the propagation direction and B (e.g., Kaminker, Pavlov, & Shibanov 1982). The two modes interact with each other via scattering. Vectors e_j for a fully ionized plasma have been derived by Shafranov (1967). Ventura (1979) gave an instructive analysis of the plasma polarization modes relevant to the neutron stars. Gnedin & Pavlov (1973) formulated the radiative transfer problem in terms of these modes. They introduced the convenient real parameters q and p, which completely determine the normal-mode polarization properties, and which are defined as

$$q + ip = \frac{\varepsilon_{yy} - \varepsilon_{xx}\cos^2\theta_B + \varepsilon_{xz}\sin 2\theta_B - \varepsilon_{zz}\sin^2\theta_B}{2i\left(\varepsilon_{xy}\cos\theta_B + \varepsilon_{yz}\sin\theta_B\right)}, \quad (25)$$

where ε_{ij} are the components of the complex permittivity tensor (Ginzburg 1970), and the z-axis is directed along B. The parameter q determines the ellipticity of the normal modes, and the parameter p is associated with absorption of radiation. In the most common case, one has

$$|q| \gg |p|, \quad q(\omega, \theta_B) \approx \tilde{q}(\omega)\frac{\sin^2\theta_B}{2\cos\theta_B}. \quad (26)$$

These relations may be invalid in narrow frequency ranges where resonant absorption occurs (e.g., near the electron or ion cyclotron resonance).

The formulae for e_j that take into account contribution of the plasma ions, implied in Shafranov (1967), have been explicitly written by Ho & Lai (2001). The electron-positron vacuum polarization in a strong magnetic field dramatically changes the normal-mode properties in certain ρ-ω domains (for a review see Pavlov & Gnedin 1984). The vacuum dielectric tensor has been obtained by Adler (1971) at $B \ll B_r$ and by Heyl & Hernquist (1997a, 1997b) in both limits of $B \ll B_r$ and $B \gg B_r$. Using these results, Ho & Lai (2003) derived convenient expressions for the polarization vectors of normal modes, which take into account the contributions from the electrons, ions, and vacuum.

The presence of bound species modifies the complex permittivity tensor and hence the properties of the normal modes. Their accurate treatment in a partially ionized medium with a strong magnetic field is a complicated problem, which has not been solved yet. The normal polarization modes of a neutral gas of hydrogen atoms in strong magnetic fields were studied by Bulik & Pavlov (1996), who applied the Kramers-Kronig relations to the bound-free and bound-bound atomic absorption coefficients obtained previously by Potekhin & Pavlov (1993) and Pavlov & Potekhin (1995). The thermal motion effects, which had not been calculated by that time for the bound-free transitions

in strong magnetic fields, were evaluated using a perturbation approximation (Pavlov & Mészáros 1993). The qualitative behavior of the polarization vectors proved to be the same as for the fully ionized plasma in a wide range of ω and θ_B, where equation (26) holds. However, there are quantitative differences. The frequencies at which equation (26) is not valid are of the order of the photoionization threshold ω_{th} and the principal bound-bound transition frequencies, where the resonant absorption takes place in the neutral gas (instead of ω_{ce} and ω_{cp} in the fully ionized plasma). The numerical values of $\tilde{q}(\omega)$ are modified. For instance, at ω well above ω_{th}, $\tilde{q}(\omega)$ is larger than it would be in the case of full ionization, which makes the normal-mode polarization more linear.

Polarization properties of normal modes in a *partially* ionized plasma with a strongly quantizing magnetic field remain unexplored. Hereafter we consider mostly situations in which the neutral fraction is small. Since even for completely nonionized gas the properties of the polarization vectors (in particular, their dependence on θ_B) are qualitatively the same as for the fully ionized plasma (except for the resonant absorption frequency ranges), we assume that the polarization modes for the fully ionized plasma are a good approximation and adopt the formulae given by Ho & Lai (2003).

At a fixed photon frequency ω, the absorption opacity $\kappa_j^a(\theta_B)$ in each mode j and scattering opacities $\kappa_{jj'}^s(\theta_B)$ from mode j into mode j' can be presented as (e.g., Kaminker et al. 1982)

$$\kappa_j^a(\theta_B) = m_H^{-1} \sum_{\alpha=-1}^{1} |e_{j,\alpha}(\theta_B)|^2 \sigma_\alpha^a , \qquad (27)$$

$$\kappa_{jj'}^s(\theta_B) = \frac{3}{4} \sum_{\alpha=-1}^{1} |e_{j,\alpha}(\theta_B)|^2 \frac{\sigma_\alpha^s}{m_H} \int_0^\pi |e_{j',\alpha}(\theta_B')|^2 \sin\theta_B' \, d\theta_B' , \qquad (28)$$

where $\alpha = 0, \pm 1$, $e_{j,0} = e_{j,z}$ is the z-component of e_j, and $e_{j,\pm 1} = (e_{j,x} \pm e_{j,y})/\sqrt{2}$ are the circular components. The cross sections σ_α depend on ω, but not on j or θ_B.

The total scattering opacity from mode j is $\kappa_j^s = \kappa_{j1}^s + \kappa_{j2}^s$, and the total extinction opacity is $\kappa_j = \kappa_j^a + \kappa_j^s$.

In the *diffusion approximation* (whose accuracy was studied, e.g., by Shibanov & Zavlin 1995), the effective opacity is

$$\kappa_j^{eff} = \left(\frac{\cos^2\vartheta}{\kappa_j^\parallel} + \frac{\sin^2\vartheta}{\kappa_j^\perp} \right)^{-1} , \qquad (29)$$

where ϑ is the angle between B and the intensity gradient,

$$\frac{1}{\kappa_j^\parallel} = \frac{3}{4} \int_0^\pi \frac{\cos^2\theta_B}{\kappa_j(\theta_B)} \sin\theta_B \, d\theta_B, \quad \frac{1}{\kappa_j^\perp} = \frac{3}{2} \int_0^\pi \frac{\sin^3\theta_B}{\kappa_j(\theta_B)} d\theta_B . \qquad (30)$$

The effective opacity for the nonpolarized radiation is $\kappa^{eff} = 2/[(\kappa_1^{eff})^{-1} + (\kappa_2^{eff})^{-1}]$.

In a partially ionized atmosphere, the opacity is contributed by electrons, ions, and bound species. The scattering cross section includes contributions from the electrons and protons: $\sigma_\alpha^s = \sigma_\alpha^{s,e} + \sigma_\alpha^{s,p}$ (the Rayleigh scattering by atoms can be important only at lower photon energies than

considered in this paper). The absorption cross section σ_α^a includes contributions from absorption by plasma electrons and protons (free-free transitions due to the electron-proton collisions, σ_α^{ff}, and proton-proton collisions, σ_α^{pp}), transitions between discrete states of an atom (bound-bound absorption, σ_α^{bb}), and photoionization (bound-free, σ_α^{bf}). Hence, for the hydrogen atmosphere we can write

$$\sigma_\alpha^a = x_H(\sigma_\alpha^{bb} + \sigma_\alpha^{bf}) + (1 - x_H)(\sigma_\alpha^{ff} + \sigma_\alpha^{pp}) , \qquad (31)$$

where x_H is the number fraction of atoms, which will be evaluated in the following section.

3. EQUATION OF STATE

3.1. *Calculation of Tables*

Our treatment of the ionization equilibrium and EOS of hydrogen in strong magnetic fields is based on the theory developed in Paper I and briefly exposed in § 2.2. Since our free-energy model is computationally expensive, it is not possible to use the EOS code "on-line" in any practical application. The alternative is to tabulate thermodynamic quantities covering the density, temperature, and magnetic field domain of interest and to rely on an interpolation procedure in the table. Here we present EOS tables that cover a range of ρ, T, and B appropriate for most typical neutron stars, such as isolated pulsars.

As discussed in Paper I, our model becomes less reliable at relatively low T and high ρ, particularly because of formation of molecules and chains H_n, which are treated in an approximate manner. In this domain, the partial number fractions and thermodynamic quantities are strongly model dependent. However, this domain of uncertainty is unimportant for modeling of not too cold neutron stars because the temperature grows inside the stellar envelope. For this reason, we have chosen as an input parameter the "astrophysical density parameter" $R = \rho_0/T_6^3$, which is customary in the stellar opacity calculations (e.g., Seaton et al. 1994; Iglesias & Rogers 1996), and restricted the calculation to $R < 4 \times 10^3$.

3.2. *Ionization Equilibrium*

Our detailed thermodynamic model shows that a strong magnetic field generally increases the fraction of bound species. In Figure 1, ionization equilibrium curves at $B = 10^{12}$ and $10^{13.5}$ G are compared with the case of $B = 0$. The latter case is treated in the framework of the nonmagnetic free-energy model (§ II of Paper I), which is a variant of the Saumon & Chabrier (1991, 1992) model. In all cases, the excited atoms contribute significantly at low ρ. In the strong magnetic field, the population of decentered atoms is also significant at low ρ. At higher density, the excluded-volume effect eliminates the excited and decentered atoms. At these high densities, the plasma species strongly interact, which leads to appearance of a significant fraction of clusters. Such clusters contribute to the EOS similarly to the atoms, lowering the pressure, but their radiation absorption properties are clearly different from those of an isolated atom. Therefore, they should be excluded from x_H in equation (31). Analogously, at low ρ we should not include in x_H the highly excited states that do not satisfy the Inglis & Teller (1939) criterion of spectral line merging, being strongly perturbed by plasma microfields. Such states form the so-called optical
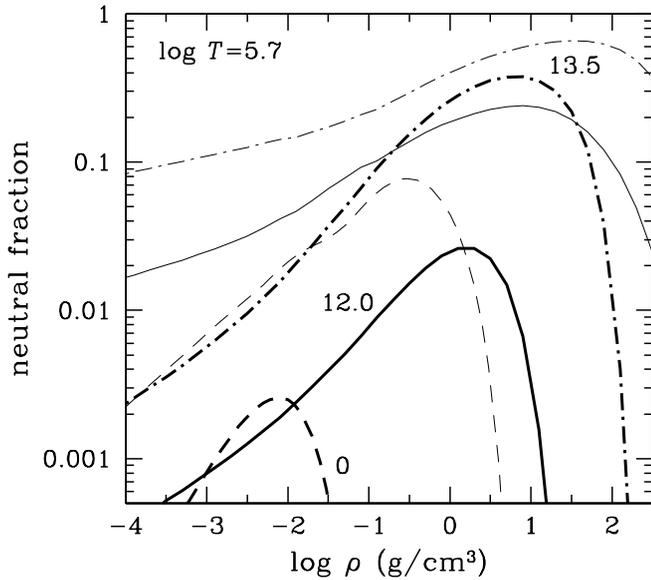
FIG. 1.—Neutral fraction of ground-state H atoms (*heavy lines*) and the total neutral fraction (including excited states and states forming the optical pseudocontinuum; *light lines*) as function of density at $T = 5 \times 10^5$ K and $B = 0$ (*dashed lines*), 10^{12} (*solid lines*), and $10^{13.5}$ G (*dot-dashed lines*).

pseudocontinuum (e.g., Däppen, Anderson, & Mihalas 1987). This distinction between the "thermodynamic" and "optical" neutral fraction is inevitable in the chemical picture of a plasma at high densities (see, e.g., Potekhin 1996b for a discussion). We discriminate the atoms that keep their identity from the "dissolved" states (i.e., strongly perturbed by the plasma environment) using the occupation probability formalism. At every s, ν, and $K_\perp$, we calculate the "optical" occupation probability $w_{\nu s}^o(K_\perp)$, replacing the Inglis-Teller criterion by an approximate criterion based on the average atomic size (eq. [14] of Pavlov & Potekhin 1995). The fraction of weakly perturbed atoms, which contribute to the bound-bound and bound-free opacities, constitutes a fraction $w_{\nu s}^o(K_\perp)/w_{\nu s}^t(K_\perp) < 1$ of the total number of atoms. Here $w_{\nu s}^t(K_\perp)$ is the "thermodynamic" occupation probability derived from the free energy (Paper I). Thick lines in Figure 1 show the neutral fraction of the

weakly perturbed atoms in their ground state, which contribute to the opacities as isolated atoms, whereas the thin lines show the total fraction of protons bound in atoms or clusters.

According to our model, at relatively low T, pressure ionization proceeds via a first-order phase transition. This "plasma phase transition" occurs at temperatures below $T_c \approx 3 \times 10^5 B_{12}^{0.39}$ K at densities around $\rho_c \approx 143 B_{12}^{1.18}$ g cm^{-3} (Paper I). In general, the validity of the free-energy models in the framework of the chemical picture of plasmas is questionable near the plasma phase transition domain. However, the T_c and ρ_c values correspond to $\log_{10} R_c \approx 3.7$, which is beyond the upper R limit for our tables, so that the plasma phase transition is not crossed along the tabulated isotherms.

Figure 2 shows the domains of partial ionization in the T-ρ plane at three values of B. With increasing B, the domains where the atomic fraction is above a specified level expand significantly. For instance, at $B = 5 \times 10^{12}$ G, the domain where $x_H > 0.01$ extends to $T = 10^6$ K. Such an amount of atoms can give an important contribution to radiative opacities.

Our tables provide values of x_H, as well as the fractions of ground-state atoms, molecules, and clusters at every R, T, and B entry.

3.3. *Thermodynamic Functions*

Figure 3 shows pressure P along two isotherms for the same field strengths as in Figure 1. The pressure varies over many orders of magnitude in the shown density range. Therefore, in order to make the discussed effects more visible, we plot in Figure 3 the *ratio* of P to $n_0 k_B T$, the pressure of an ideal monatomic hydrogen gas at the same ρ and T.

At different field strengths (including $B = 0$), the deviations from the ideal gas behavior are qualitatively the same, but quantitatively different. At very low ρ, we have nearly fully ionized, almost ideal nondegenerate gas of electrons and protons, so that $P/n_0 k_B T \approx 2$. With increasing density, atomic recombination proceeds according to the Saha equation (in the strong magnetic field, the modified Saha equation is given by eq. [54] of Paper I). Therefore, the ratio $P/n_0 k_B T$ decreases. At high density, however, the atoms become pressure ionized: in this region the increase of P due
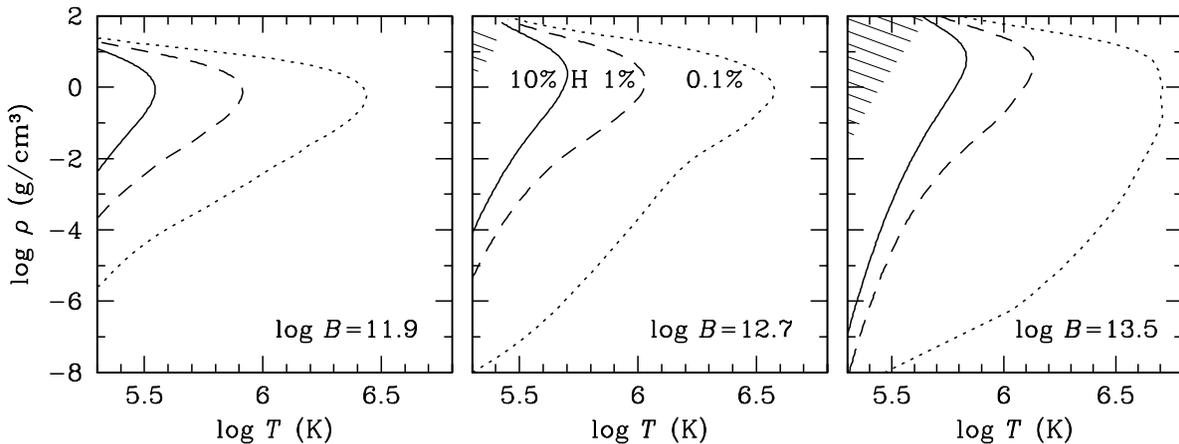

FIG. 2.—Domains of partial ionization at $\log_{10} B/\mathrm{G} = 11.9$, 12.7, and 13.5. The contours delimit the domains where the atomic fraction exceeds 0.1% (*dotted lines*), 1% (*dashed lines*), or 10% (*solid lines*). The hatched region is the domain where the molecular fraction exceeds 1%.
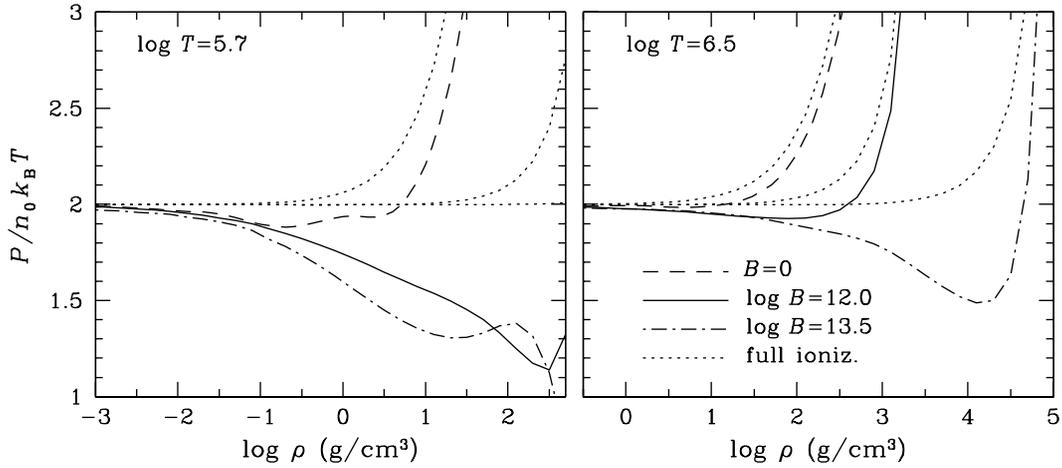
FIG. 3.—Pressure P relative to $n_0 k_B T$, where n_0 is the total number density of protons (free and bound). *Left panel*: $T = 10^{5.7}$ K; *right panel*: $T = 10^{6.5}$ K; *dashed lines*: $B = 0$, *solid lines*: $B = 10^{12}$ G, *dot-dashed lines*: $B = 10^{13.5}$ G. Dotted lines represent the pressure of a fully ionized electron-proton ideal gas at the same values of T and B.

to the increased number of free electrons and protons competes with a negative nonideal contribution, which is mainly due to the Coulomb term F_{ex}^C in the free energy. The dot-dashed curve bends down near the high-ρ edge of the left-hand panel of Figure 3 because of enhancement of the nonideal contribution; it is a precursor of the plasma phase transition, where our model becomes inapplicable. Finally, at still higher densities, the electrons become degenerate and raise the pressure far above $n_0 k_B T$. The dotted lines in Figure 3 show the pressure of an ideal electron-proton gas; their upward bending marks the onset of electron degeneracy. At $B = 0$, it occurs at $\rho \gtrsim m_H (2 m_e k_B T)^{3/2}/(3\pi^2 \hbar^3) \approx 6 T_6^{3/2}$ g cm^{-3}, but in the strongly quantizing field the electrons become degenerate at $\rho \gtrsim (m_H/\pi^2 \hbar a_m^2)(m_e k_B T/2)^{1/2} \approx 613 B_{12}\sqrt{T_6}$ g cm^{-3}.

Since the strong magnetic field enhances atomic recombination and delays pressure ionization and electron degeneracy at high densities, the discussed features of the $P/n_0 k_B T$ curves become more prominent and shift to higher ρ with increasing B, as seen in Figure 3.

Along with the pressure, our EOS tables contain internal energy U, entropy S, specific heat C_V, and the logarithmic derivatives of pressure $\chi_T = (\partial \ln P/\partial \ln T)_V$ and $\chi_\rho = -(\partial \ln P/\partial \ln V)_T$. Other second-order quantities can be calculated using the Maxwell relations (e.g., Landau & Lifshitz 1993). For example, the heat capacity at constant pressure, C_P, and adiabatic gradient, $\nabla_{ad} = (\partial \log T/\partial \log P)_S$, are given by relations

$$C_P = C_V + \frac{PV}{T}\frac{\chi_T^2}{\chi_\rho}, \quad \nabla_{ad} = \frac{\chi_T}{\chi_T^2 + \chi_\rho C_V T/(PV)} . \quad (32)$$

Figure 4 shows ∇_{ad} at different values of B. At low density, the magnetic field increases the adiabatic gradient, thus stabilizing the matter against convection. This thermodynamic effect is additional to the hydromagnetic stabilization considered, e.g., by Chandrasekhar (1961) and Miralles, Urpin, & van Riper (1997). However, at higher densities, $\rho \sim 1$–100 g cm^{-3}, there is a significant decrease of ∇_{ad} due to the partial recombination of H atoms. The adiabatic gradient increases again at still higher densities, where the plasma is fully pressure ionized.

4. CROSS SECTIONS

4.1. *Scattering*

The scattering cross sections by the electrons under the conditions typical for photospheres of the neutron stars with strong magnetic fields were thoroughly studied in the past (e.g., Ventura 1979; Kaminker et al. 1982; Mészáros 1992 and references therein). The cross section $\sigma_{-1}^{s,e}$ exhibits a resonance at the electron cyclotron frequency ω_{ce}. Outside of a narrow (about the Doppler width) frequency range around ω_{ce}, the cross sections are

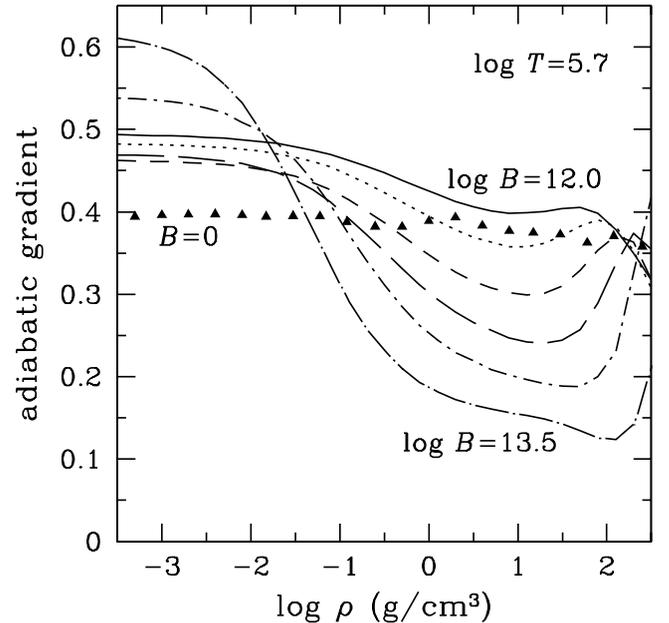$$\sigma_\alpha^{s,e} = \frac{\omega^2}{(\omega + \alpha\omega_{ce})^2 + \nu_{e,\alpha}^2}\sigma_T , \quad (33)$$

FIG. 4.—Adiabatic temperature gradient ∇_{ad} at $T = 5 \times 10^5$ K, for different field strengths (shown by different line styles): $\log_{10} B/G = 12.0$, 12.3, 12.6, 12.9, 13.2, and 13.5. Triangles show the zero-field case.

where $\sigma_{\rm T} = (8\pi/3)(e^2/m_e c^2)^2$ is the nonmagnetic Thomson cross section and $\nu_{e,\alpha}$ is an effective damping frequency given by equation (38) below.

The scattering by the protons, which is completely negligible in a nonmagnetized plasma, becomes important in the strong magnetic field, because $\sigma_{+1}^{s,p}$ exhibits a resonance at $\omega_{\rm cp}$. It is the same as the electron cyclotron resonance but a different mass and opposite charge of the particle:

$$\sigma_\alpha^{s,p} = \left(\frac{m_e}{m_p}\right)^2 \frac{\omega^2}{(\omega - \alpha\omega_{\rm cp})^2 + \nu_{p,\alpha}^2}\sigma_{\rm T} . \qquad (34)$$

The damping frequency $\nu_{p,\alpha}$ will be derived below (eq. [53]).

We neglect the Doppler broadening of these resonances. Within the thermal width of the cyclotron resonance, the treatment of radiation scattering is nontrivial (e.g., Ventura et al. 1985 and references therein). However, at $T \lesssim 10^7$ K, the Doppler width $\sim \omega(T/T_r)^{1/2}$ is smaller than the frequency resolution of our opacity tables (chosen to be $\Delta \log_{10} \omega = 0.02$).

4.2. Absorption by Atoms

Oscillator strengths for the H atom which rests in a strong magnetic field were calculated, e.g., by Forster et al. (1984). Bound-bound transitions of the H atom moving arbitrarily in a strong magnetic field were studied by Pavlov & Potekhin (1995). The modification of the binding energies due to the atomic motion (§ 2.1) leads to a dramatic "magnetic broadening" of the spectral lines averaged over all states of motion, which exceeds by orders of magnitude the usual Doppler broadening. Thus the spectral profile of the bound-bound opacities becomes continuous in a wide frequency range, resembling a reversed bound-free profile. Our calculation of the bound-bound absorption cross sections relies on the theory presented by Pavlov & Potekhin (1995) and employs fitting formulae for the binding energies, oscillator strengths, and electron collision widths derived by Potekhin (1998).

Photoionization cross sections of the nonmoving H atom in a magnetic field were calculated by many authors (e.g., Potekhin, Pavlov, & Ventura 1997 and references therein). Photoionization of the H atom in a strong magnetic field with allowance for motion was studied, using different modifications of the adiabatic approximation (§ 2.1) by Bezchastnov & Potekhin (1994) and Kopidakis, Ventura, & Herold (1996). A complete numerical treatment beyond the adiabatic approximation has been developed by Potekhin & Pavlov (1997), who adapted the **R**-matrix formalism (Wigner & Eisenbud 1947) to the case under study. They showed that none of the versions of the adiabatic approximation can provide accurate $\sigma_\alpha^{\rm bf}$ for all values of α and $K_\perp$, particularly because the continuum-channel coupling strongly affects $\sigma_\pm^{\rm bf}$ at sufficiently large $K_\perp$. Here we use the complete numerical treatment. Since it is computationally involved, we use an interpolation across a precalculated set of tables. For each of the three basic polarizations, we have calculated $\sigma_\alpha^{\rm bf}(\omega, K_\perp, B)$ on a predefined grid, with $\log_{10} \hbar\omega$ (eV) ranging from 1.0 to 4.5 with step 0.02, $\log_{10} K_\perp$ (a.u.) ranging from 1 to 3 with step 0.1, and $\log_{10} B$ (G) ranging from 11.9 to 13.5 with step 0.1. At the low-$K_\perp$ end of the grid, $K_\perp = 10$ a.u., the atomic properties are virtually the same as at $K = 0$; beyond the upper limit, $K_\perp > 10^3$ a.u.,

the contribution of the bound-free transitions to the total opacities is negligible. The grid is sufficiently fine for calculation of atmosphere models. However, the step 0.02 in $\log_{10} \omega$ does not allow us to resolve the narrow Beutler-Fano–type resonances which appear due to autoionizing states in the vicinity of photoionization thresholds of partial cross sections (Potekhin et al. 1997; Potekhin & Pavlov 1997). Whenever such a resonance occurs near a grid point, it produces a spurious outlier on the otherwise smooth $\sigma_\alpha^{\rm bf}(\omega, K_\perp)$ dependence. We filter out such outliers by smoothing $\sigma_\alpha^{\rm bf}$ as a function of ω at every $K_\perp$, using the three-point median filter. Since the grid does not allow us to resolve the photoionization threshold accurately, the threshold frequency $\omega_{\rm th}$ is determined independently for every $K_\perp$, using analytic fits to the binding energies (Potekhin 1998).

In addition to the bound-bound and bound-free atomic transitions, in a plasma environment there are transitions from bound states to the highly perturbed atomic states discussed in § 3.2. These perturbed levels effectively dissolve and merge in a pseudocontinuum, which lies below the photoionization threshold. In order to take into account the radiative transitions into this pseudocontinuum, we employ a below threshold extrapolation, as described for the zero-field case by Däppen et al. (1987), Stehlé & Jacquemot (1993), and Seaton et al. (1994). Below $\omega_{\rm th}$, the effective "bound–quasi-free" photoabsorption cross section due to the dissolved lines is

$$\sigma_\alpha^{\rm bf}(\omega < \omega_{\rm th}) = \frac{2\pi e^2}{m_e c}\frac{w_i^o - w_f^o}{w_i^o}f_{if,\alpha}\frac{d\nu_f}{d\omega} , \qquad (35)$$

where w_i^o and w_f^o are the optical occupation probabilities of the initial and final states, respectively, $f_{if,\alpha}$ is the corresponding oscillator strength, and $d\nu_f/d\omega$ is the number of final states per unit frequency interval. By analogy with Stehlé & Jacquemot (1993), we interpolate w_f^o as function of frequency and set $w_f^o = w_i^o$ at ω smaller than the lowest allowed transition frequency. Taking into account that $\sigma_\alpha^{\rm bf}(\omega < \omega_{\rm th})$ is a smooth continuation of $\sigma_\alpha^{\rm bf}(\omega > \omega_{\rm th})$ (Däppen et al. 1987), we write

$$\sigma_\alpha^{\rm bf}(K_\perp, \omega < \omega_{\rm th}) = \left[1 - \frac{w_f^o(K_\perp, \omega)}{w_i^o(K_\perp)}\right]\sigma_\alpha^{\rm bf,extr}(K_\perp, \omega) , \qquad (36)$$

where $\sigma_\alpha^{\rm bf,extr}(K_\perp, \omega)$ is a power-law extrapolation of $\sigma_\alpha^{\rm bf}(K_\perp, \omega)$ at $\omega < \omega_{\rm th}$.

Unlike the $B = 0$ case, in our case $f_{if,\alpha}$ and w_f^o depend on polarization. For photoabsorption by an atom in the ground state, $f_{if,\pm 1} \neq 0$ only for even upper states, whereas $f_{if,0} \neq 0$ only for odd states. We take into consideration only the appropriate states while calculating w_f^o in equation (36).

The $K_\perp$-dependent cross sections are averaged over the distribution of atoms over $K_\perp$ with statistical weights $w_i^o(K_\perp) \exp[-\epsilon_i(K_\perp)/k_{\rm B}T]$, as in Pavlov & Potekhin (1995) and Potekhin & Pavlov (1997).

4.3. Free-Free Absorption

In the classical cold plasma approximation (e.g., Ginzburg 1970), the free-free absorption by electrons is

$$\sigma_\alpha^{\rm ff} = \frac{1}{(\omega + \alpha\omega_{\rm ce})^2 + \nu_{e,\alpha}^2}\frac{4\pi e^2}{m_e c}\nu_\alpha^{\rm ff}(\omega) , \qquad (37)$$

where ν_α^{ff} is an effective frequency of electron-proton collisions which lead to absorption of photons. Broadening of the electron cyclotron resonance in equations (33) and (37) is determined by the sum of the effective frequencies for absorption and scattering,

$$\nu_{e,\alpha} = \nu_\alpha^{\mathrm{ff}} + \nu_e^s , \qquad (38)$$

where

$$\nu_e^s = \frac{2}{3}\frac{e^2}{m_e c^3}\omega^2 \qquad (39)$$

is the natural (radiative) width of the resonance. The damping frequency given by equation (38) ensures the correct value of the cyclotron absorption cross section integrated across the resonance (e.g., Ventura 1979):

$$\int_{\omega_{ce}-\Delta\omega}^{\omega_{ce}+\Delta\omega}\left[\sigma_{-1}^{s,e}(\omega)+\sigma_{-1}^{\mathrm{ff}}(\omega)\right]d\omega = \frac{4\pi^2 e^2}{m_e c} , \qquad (40)$$

with $\nu_{e,\alpha} \ll \Delta\omega \ll \omega_{ce}$.

The values of ν_α^{ff} are provided by quantum mechanical calculations. It is customary (e.g., Armstrong & Nicholls 1972) to express σ^{ff} through the thermally averaged Gaunt factors $\bar{g}$ or, equivalently, Coulomb logarithms $\Lambda = (\pi/\sqrt{3})\bar{g}$. Taking into account equation (37), we can write

$$\nu_\alpha^{\mathrm{ff}} = \frac{4}{3}\sqrt{\frac{2\pi}{m_e k_{\mathrm{B}} T}}\frac{n_e e^4}{\hbar\omega}(1-e^{-u})\Lambda_\alpha^{\mathrm{ff}}, \quad u \equiv \frac{\hbar\omega}{k_{\mathrm{B}} T} . \qquad (41)$$

The factor $(1-e^{-u})$ allows for the induced radiation.

4.3.1. Infinite Proton Mass Approximation

In the zero-field case, the electron free-free absorption rate can be calculated assuming the electron scattering off a fixed Coulomb potential. In this case, allowance for the finite ion mass consists of replacing m_e by the reduced mass μ. The Born approximation yields the well-known formula for the cross section of free-free photoabsorption by an electron having an initial momentum p_i and final momentum $p_f = (p_i^2 + 2m_e\hbar\omega)^{1/2}$ (e.g., Bethe & Salpeter 1957),

$$\sigma^{\mathrm{ff}}(p_i,\omega) = \frac{16\pi^2 n_e e^6}{3m_e c\hbar\omega^3}\frac{1}{p_i}\ln\left|\frac{p_f + p_i}{p_f - p_i}\right| , \qquad (42)$$

whose averaging over the Maxwell distribution gives the classical Coulomb logarithm

$$\Lambda_{\mathrm{cl}}^{\mathrm{ff}} = e^{u/2}K_0\left(\frac{u}{2}\right) , \qquad (43)$$

$K_0(u/2)$ being the modified Bessel function. Hummer (1988) calculated $\bar{g}^{\mathrm{ff}}$ using accurate non-Born quantum mechanical results by Karzas & Latter (1961) and fitted it by a Padé formula. The nonmagnetic Gaunt factor is applicable if the magnetic field is nonquantizing, i.e., if $\beta_e < 1$, where β_e is given by equation (1). In the quantizing magnetic fields, the Coulomb logarithm was evaluated in the Born approximation by several authors (Pavlov & Panov 1976; Nagel 1980; Mészáros 1992). In this approximation, $\Lambda_\alpha^{\mathrm{ff}}$, which is generally a function of B, T, and ω, depends only on the two

dimensionless arguments, u and β_e:[1]

$$\Lambda_\alpha^{\mathrm{ff}} = \tfrac{3}{4}e^{u/2}\sum_{n=-\infty}^{\infty}\int_0^{\infty}Q_n^\alpha(\beta_e,u,y)dy , \qquad (44a)$$

where

$$Q_n^\alpha(\beta_e,u,y) = \frac{y}{\zeta}\frac{A_n^\alpha}{[(y+\theta+\zeta)\sinh(\beta_e/2)]^{|n|}} , \qquad (44b)$$

$$A_n^0 = \frac{x_n K_1(x_n)}{y+\beta_e/4}, \quad A_n^{\pm 1} = \frac{y+\theta+|n|\zeta}{\zeta^2}K_0(x_n) , \qquad (44c)$$

$$\zeta = \sqrt{1+2\theta y + y^2}, \quad \theta = \frac{1+\exp(-\beta_e)}{1-\exp(-\beta_e)} , \qquad (44d)$$

$$x_n = |u-n\beta_e|\sqrt{0.25+\frac{y}{\beta_e}} . \qquad (44e)$$

Equations (44a)–(44e) have been derived assuming that an electron scatters off a fixed Coulomb center. Actually the protons are moving and can absorb radiation during collisions. Although this process is negligible at $B = 0$, it may be important at ω near or below ω_{cp}. The previous authors (Pavlov et al. 1995; Zane et al. 2000, 2001; Özel 2001; Ho & Lai 2001) supplemented $\sigma_\alpha^{\mathrm{ff}}$ by a cross section of "ion free-free absorption," $\sigma_\alpha^{\mathrm{ff},p}$. For hydrogen, taking into account equations (33) and (34), their formulae can be written as

$$\sigma_\alpha^a = \sigma_\alpha^{\mathrm{ff}} + \sigma_\alpha^{\mathrm{ff},p}, \quad \frac{\sigma_\alpha^{\mathrm{ff},p}}{\sigma_\alpha^{s,p}} = \frac{\sigma_\alpha^{\mathrm{ff}}}{\sigma_\alpha^{s,e}} . \qquad (45)$$

We find, however, that equation (45) is erroneous.

4.3.2. Absorption in Proton Collisions

There are two effects of the finite proton mass on the absorption: first, the absorption can occur in proton-proton collisions, and second, the absorption in the electron-proton collisions is modified because of the proton motion. Let us start with the first process. By analogy with equation (37), we write the cross section as

$$\sigma_\alpha^{pp} = \frac{1}{(\omega - \alpha\omega_{cp})^2 + \nu_{p,\alpha}^2}\frac{4\pi e^2}{m_p c}\nu_\alpha^{pp}(\omega) , \qquad (46)$$

where ν_α^{pp} is the effective frequency to be determined.

In the classical picture (Ginzburg 1970), an ion-ion collision does not change the total electric current and hence does not cause dissipation. Therefore, it does not contribute to the damping of radiation. In quantum mechanics, this corresponds to vanishing dipole matrix element for the absorption. In Appendix A we evaluate the nonvanishing quadrupole term under the condition that the magnetic field does not quantize proton motion, that is, $\beta_p < 1$, and obtain

$$\nu^{pp} = \frac{256}{3}\sqrt{\frac{\pi}{m_p k_{\mathrm{B}} T}}\frac{n_p e^4}{\hbar\omega}\frac{k_{\mathrm{B}} T}{m_p c^2}(1-e^{-u})\Lambda_{pp} , \qquad (47)$$

where Λ_{pp} is an appropriate Coulomb logarithm. In Figure 5, Λ_{pp} is plotted by the solid line. For comparison, we also show Λ for distinguishable particles (corresponding to eq. [A4]; dashed line), and the classical Coulomb logarithm

---

[1] The set of equations given by eq. (44) is equivalent to eq. (27) of Pavlov & Panov (1976), but in eq. (44c) for $A_n^{\pm 1}$ we have restored the power 2 of ζ, lacking in Pavlov & Panov (1976) apparently due to a misprint.
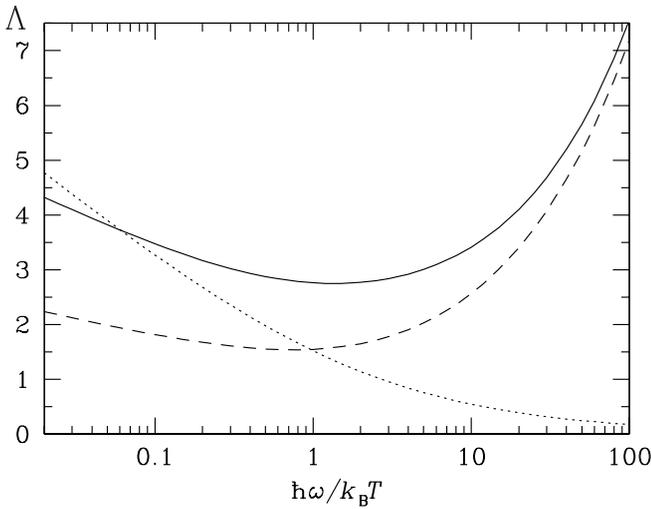
FIG. 5.—Coulomb logarithms for photoabsorption in collisions of non-relativistic protons (Λ_{pp}, *solid line*), collisions of identical but distinguishable particles (*dashed line*), and electron-proton scattering (Λ_{cl}^{ff}, *dotted line*).

Λ_{cl}^{ff} (eq. [41]; *dotted line*). The fit

$$\Lambda_{pp} \approx 0.6 \ln\left(22u^{-1} + 9u^{-0.3}\right) + 0.4\sqrt{\pi u} \qquad (48)$$

accurately reproduces Λ_{pp} at small and large u and has a maximum error within 1.5% at intermediate u.

We see that σ_α^{pp} differs from $\sigma_\alpha^{ff,p}$ (defined by eq. [45] with the use of eqs. [37] and [41]) by a factor of $32(2m_p/m_e)^{1/2} \times (k_B T/m_p c^2)\Lambda_{pp}/\Lambda_{cl}^{ff} \sim T/10^9$ K.

One should remember that equations (46)–(48) are obtained in the nonrelativistic approximation. Therefore they do not take into account spin-flip processes and are inapplicable at very high T or high ω, where the relativistic corrections can be important.

4.3.3. *Electron Free-Free Process with Allowance for Finite Proton Mass*

Let us write the cross section of photoabsorption due to the electron-proton collisions in the form of combined equations (37) and (41), neglecting broadening:

$$\sigma_\alpha^{ff} = \frac{2^{9/2}\pi^{3/2}n_e e^6}{3m_e^{3/2}(k_B T)^{1/2}c\hbar\omega}\frac{1-e^{-u}}{(\omega+\alpha\omega_{ce})^2}\Lambda_\alpha^e. \qquad (49)$$

The superscript "e" indicates that the electron (not proton) cyclotron resonance has been separated off Λ_α. Since the colliding electron and proton are treated on equal footing, we anticipate that thus defined *normalized cross section* Λ_α^e will reveal a resonant peak at $\omega \sim \omega_{cp}$.

The initial and final states of the interacting electron and proton are just continuum states of the H atom. An accurate treatment of these states would imply a solution of the coupled channel equations given by equation (15) and calculation of the **R**-matrix, as we did for the bound-free process. However, we will restrict to the first Born approximation. In this approximation, Λ_α^e is given by equations (B20)–(B22) derived in Appendix B. For the longitudinal polarization ($\alpha = 0$), a calculation by these equations well reproduces the Coulomb logarithm (42) obtained in the infinite proton mass approximation. However, for the two circular polarizations the result is different; it is shown in
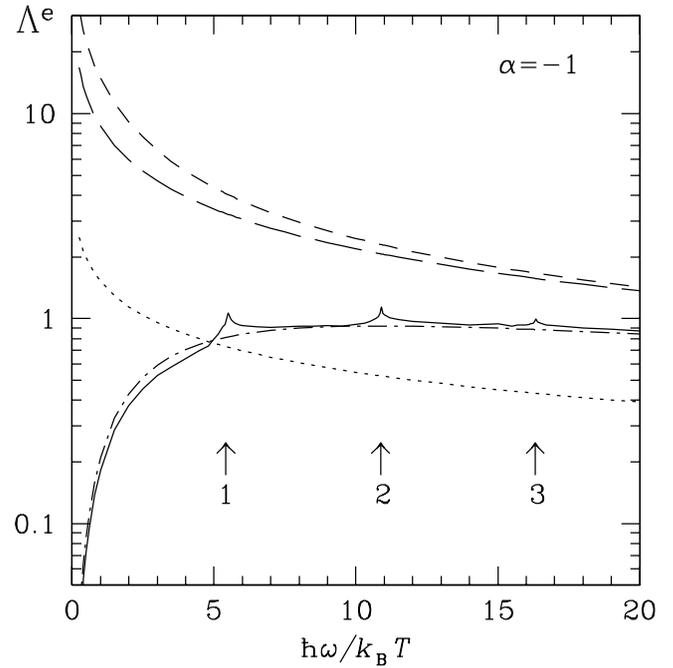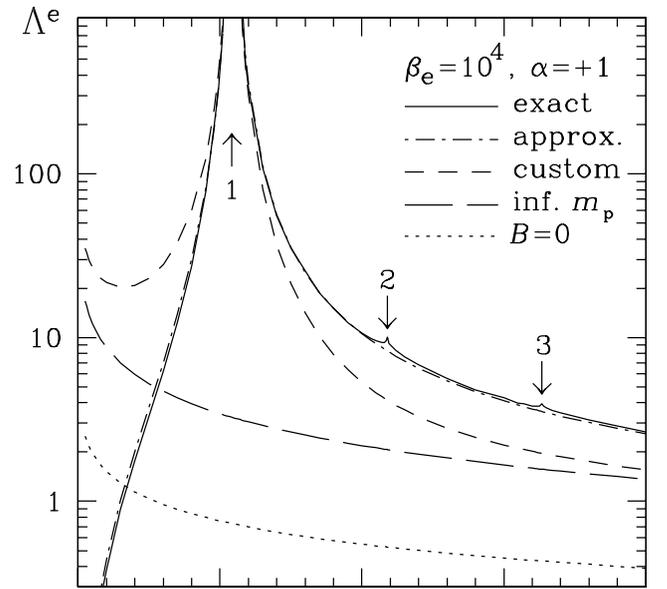

FIG. 6.—Comparison of accurate and approximate normalized free-free cross sections Λ_α^e (eq. [49]) for two circular polarizations $\alpha = \pm 1$ at $\beta_e = 10^4$. *Solid lines*: eqs. (B19)–(B22); *dot-dashed lines*: eq. (51); *short-dashed lines*: customary approximation, eq. (45); *long-dashed lines*: Λ_α^{ff}, eq. (44); *dotted lines*: Λ_{cl}^{ff}, eq. (43). Arrows indicate the proton cyclotron harmonics.

Figure 6 by the solid lines. As expected, we see a remarkable proton cyclotron resonance at $\alpha = +1$, which is due to the denominator $\omega - \omega_{cp}$ in the last terms of equation (B22c). In addition, for both circular polarizations there are smaller spikes at higher proton-cyclotron harmonics, arising from the logarithmic singularities of $\tilde{v}_{nsn's}(\rho, \kappa)$ at $\kappa \to 0$ (see eq. [B8]). Apart from these spikes, Λ_{+1}^e is accurately described by the formula $\Lambda_{\pm 1}^e \approx \Lambda_{\pm 1}^{ff}\omega^2/(\omega - \alpha\omega_{cp})^2$, where $\Lambda_{\pm 1}^{ff}$ is given by equation (44) (Fig. 6, *dot-dashed lines*). We note that the factor $\omega^2/(\omega - \alpha\omega_{cp})^2$ naturally appears in the classical plasma model with allowance for the ion motion. The classical model also helps to restore the damping factors

neglected in equation (49). Let ν_e and ν_p be the electron and proton damping frequencies due to processes other than the electron-ion collisions. For the processes considered above (Thomson scattering and proton-proton collisions),[2] we have $\nu_e = \nu_e^s$ and $\nu_p = \nu_p^s + \nu^{pp}$, where $\nu_p^s = 2e^2\omega^2/(3m_p c^3)$ is the natural width of the proton cyclotron resonance. Averaged Newtonian equations of motion for the electrons and protons in the magnetic and radiation fields give the complex permittivity tensor ε (cf. Ginzburg 1970, § 10). Neglecting $(m_e/m_p)^{1/2}$ compared to unity and assuming that $\nu_p \ll \nu_e \ll \omega$, we have

$$\text{Im}(\varepsilon_{xx} + i\alpha\varepsilon_{xy})$$

$$= \frac{\omega_{\text{pl}}^2}{\omega}\left[\omega_{\text{cp}}(\omega_{\text{ce}} + \alpha\omega)\nu_p + \omega(\omega - \alpha\omega_{\text{cp}})\nu_e + \omega^2\nu_\alpha^{\text{ff}}\right]$$

$$\times \left\{\left[(\omega + \alpha\omega_{\text{ce}})(\omega - \alpha\omega_{\text{ce}}) - \nu_\alpha^{\text{ff}}\left(\nu_p + \nu_e\frac{m_e}{m_p}\right) - \nu_p\nu_e\right]^2\right.$$

$$\left. + \left[\omega\nu_\alpha^{\text{ff}} + (\omega + \alpha\omega_{\text{ce}})\nu_p + (\omega - \alpha\omega_{\text{cp}})\nu_e\right]^2\right\}^{-1},$$

$$(50)$$

where $\alpha = \pm 1$ and Im means the imaginary part. Neglecting the tiny shift of the position of the cyclotron resonances caused by the damping, we can now write

$$\sigma_\alpha^{\text{ff}} \approx \frac{\omega^2}{(\omega + \alpha\omega_{\text{ce}})^2(\omega - \alpha\omega_{\text{cp}})^2 + \omega^2\tilde{\nu}_\alpha^2}\frac{4\pi e^2\nu_\alpha^{\text{ff}}}{m_e c}, \quad (51)$$

where

$$\tilde{\nu}_\alpha = \nu_\alpha^{\text{ff}} + \left(1 + \frac{\alpha\omega_{\text{ce}}}{\omega}\right)\nu_p + \left(1 - \frac{\alpha\omega_{\text{cp}}}{\omega}\right)\nu_e, \quad (52)$$

and ν_α^{ff} is given by equation (41).

The accurate calculations according to Appendix B are reproduced by equations (51) and (41), if we multiply $\Lambda_\alpha^{\text{ff}}$ in the latter equation by a correction factor of the order of unity. This quantum correction factor proves to be the same for $\alpha = +1$ and $\alpha = -1$. Thus, the two effective collision frequencies (longitudinal ν_0^{ff} and transverse $\nu_{+1}^{\text{ff}} = \nu_{-1}^{\text{ff}}$) provide the three $\sigma_\alpha^{\text{ff}}$.

Near the electron cyclotron resonance ($\omega \approx \omega_{\text{ce}}$, $\alpha = -1$), the damping frequency $\tilde{\nu}_\alpha$ approximately reproduces $\nu_{e,\alpha}$ in equation (38), which ensures the condition given by equation (40). Near the proton cyclotron resonance ($\omega \approx \omega_{\text{cp}}$, $\alpha = +1$), the effective damping frequency is $\tilde{\nu}_\alpha\omega/\omega_{\text{ce}} \approx \tilde{\nu}_\alpha m_e/m_p \approx \nu_{p,\alpha}$, where

$$\nu_{p,\alpha} = \nu_\alpha^{\text{ff},p} + \nu_p^s + \nu_\alpha^{pp}, \quad \nu_\alpha^{\text{ff},p} \equiv \frac{m_e}{m_p}\nu_\alpha^{\text{ff}}. \quad (53)$$

Equation (53) is consistent with the requirement of oscillator strength conservation for the proton cyclotron resonance in polarization $\alpha = +1$, fully analogous to equation (40).

---

[2] We do not consider the electron-electron collisions. At $B = 0$, they are known to be unimportant for the bremsstrahlung, except for relativistic energies (e.g., Bethe & Salpeter 1957). The magnetic field does not change this conclusion, because the resonance, which appears at $\omega = \omega_{\text{ce}}$ for this process, merges in the more powerful classical cyclotron resonance for the usual free-free and Thomson processes.

From the relations

$$\frac{\nu^{pp}}{\nu_\alpha^{\text{ff},p}} = 1.78 \times 10^{-4}T_6\frac{\Lambda_{pp}}{\Lambda_\alpha^{\text{ff}}}, \quad \frac{\nu^{pp}}{\nu_p^s} = \frac{3.6\rho_0}{T_6^{5/2}}\frac{1 - e^{-u}}{u^3}\Lambda_{pp}, \quad (54)$$

we see that the proton-proton collisions can be safely neglected at any T and ρ typical of outer envelopes of the neutron stars.

For comparison, Figure 6 also shows the nonmagnetic Coulomb logarithm $\Lambda_{\text{cl}}^{\text{ff}}$ (dotted lines), $\Lambda_\alpha^{\text{ff}}$ given by equation (44) (long-dashed lines), which neglects the finite proton mass, and the Λ_α^e that would correspond to the calculation of σ_α^a according to the traditional equation (45) (short-dashed lines). It is easy to see the difference of equations (49) and (51) from equation (45). The customary recipe (44) misses the interference of the first two terms in each of equations (B22b) and (B22c) (related to transitions with changing Landau number n) with the terms in square brackets (related to transitions that keep n constant). At $\omega < \omega_{\text{cp}}$, the latter terms tend to compensate the former ones. A suppression factor $\sim(\omega/\omega_{\text{cp}})^2$, which follows from equation (51) at $\omega \ll \omega_{\text{cp}}$, is brought about by this interference. From the classical physics point of view, it may be explained as follows: very slow ($\omega \ll \omega_{\text{cp}}$) oscillations of the radiation electric field, perpendicular to the constant magnetic field, make both particles, electron and proton, drift adiabatically with the velocity $(c/B^2)\boldsymbol{E} \times \boldsymbol{B}$, so that in the drifting frame of reference they do not "feel" the electric field of the electromagnetic wave. The suppression of the free-free cross sections takes place for both circular polarizations.

As is well known, the Born approximation is accurate only at $\hbar\omega$ much larger than the binding energies. In order to partly correct $\Lambda_\alpha^{\text{ff}}$ beyond this approximation and to recover the non-Born Gaunt factor $\bar{g}^{\text{ff}}$ at $B = 0$, we multiply $\Lambda_\alpha^{\text{ff}}$ by the ratio of $\bar{g}^{\text{ff}}$ (Hummer 1988) to $\bar{g}_{\text{Born}}^{\text{ff}} = (\sqrt{3}/\pi)\Lambda_{\text{cl}}^{\text{ff}}$.

5. OPACITIES

5.1. Fully Ionized Atmosphere

For a fully ionized atmosphere model, the monochromatic opacities calculated in the framework of the theory outlined in § 2.3 do not differ much from the opacities used in the previous models (e.g., Shibanov et al. 1992) at $\omega > \omega_{\text{cp}}$. However, the improved treatment of the free-free contribution results in a considerable modification of the opacities at $\omega < \omega_{\text{cp}}$. Figure 7 shows monochromatic opacities for two polarization modes, $j = 1$ (solid lines) and $j = 2$ (dashed lines) for radiation propagating at three angles θ_B with respect to the field lines. The atmosphere parameters chosen for this figure can be expected near the bottom of a magnetar photosphere: $\rho = 500$ g cm^{-3}, $T = 5 \times 10^6$ K, and $B = 5 \times 10^{14}$ G. An extension of our EOS for the superstrong magnetic fields (work currently in progress; Chabrier, Douchin, & Potekhin 2002) indicates that the model of a fully ionized atmosphere is adequate for this relatively high value of ρ. At these parameters, the proton cyclotron resonance at $\hbar\omega = 3.15$ keV is quite prominent. At small θ_B, the opacities of the two normal modes cross each other at $\omega \approx \omega_{\text{cp}}$, which is a well-known phenomenon (e.g., Shibanov et al. 1992). Another mode crossing, which occurs at $\hbar\omega \approx 7.6$ keV, is due to the vacuum resonance (e.g., Soffel et al. 1983; Pavlov & Gnedin 1984; Shibanov et al. 1992). Near the crossing points, the modes may become completely
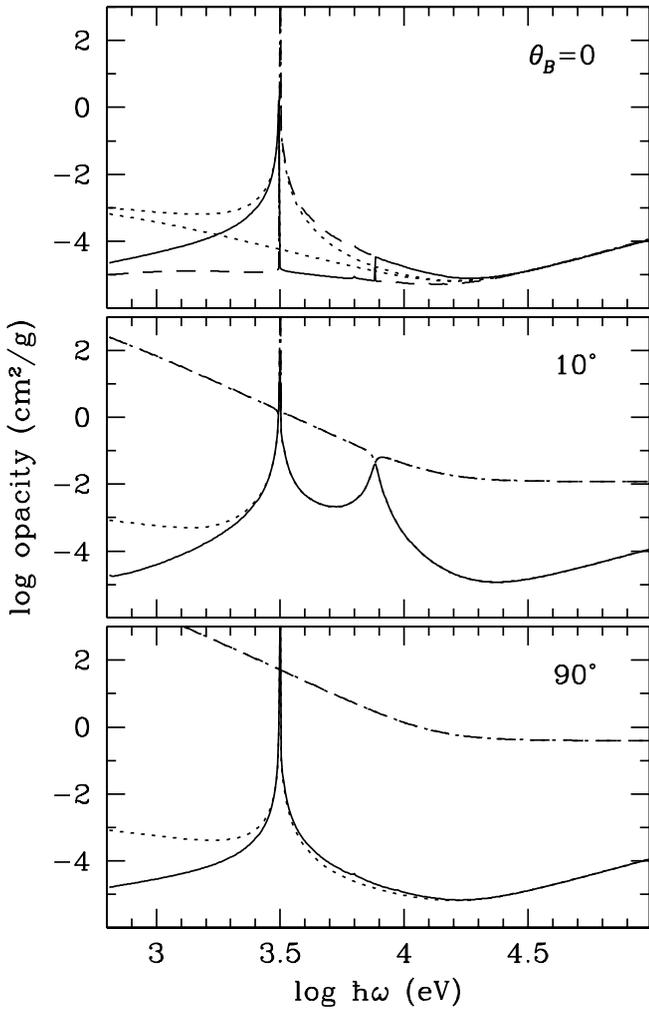
FIG. 7.—Monochromatic radiative opacities for the ordinary (*dashed lines*) and extraordinary (*solid lines*) polarization modes in a plasma at $\rho = 500$ g cm^{-3}, $T = 5 \times 10^6$ K, and $B = 5 \times 10^{14}$ G, for $\theta_B = 0°$, $10°$, and $90°$. Dotted lines show the opacities according to eq. (45). Here the opacity is calculated assuming complete ionization.

FIG. 8.—Effective opacities for diffusion of nonpolarized radiation along (*left panel*) or across (*right panel*) the magnetic field, at the same plasma parameters as in Fig. 7: new (*solid lines*) and old (*dotted lines*) results.

5.2. *Partially Ionized Atmosphere*

As follows from § 3.2, the amount of neutral hydrogen in neutron star photospheres can be significant at $T \lesssim 10^6$ K. For example, at $\rho = 0.1$ g cm^{-3}, $T = 10^{5.5}$ K, and $B = 2.35 \times 10^{12}$ G, 12% of protons are bound in the ground-state H atoms. Monochromatic opacities for this case are shown in Figure 9 for three basic polarizations. The contribution of the fully ionized plasma component is shown by dot-dashed lines, while dotted and dashed lines show bound-bound and bound-free contributions, respectively. The total opacities are plotted by the solid lines. We see that the bound-free contribution is important for any polarization, whereas the bound-bound opacity is important for $\alpha = \pm 1$ but unimportant for the longitudinal polarization ($\alpha = 0$). This is because the dipole selection rule forbids radiative transitions between different tightly bound states with absorption of a photon polarized along $\mathbf{B}$. Transitions to the odd hydrogen-like states ($\nu = 1, 3, \ldots$) are allowed, but the corresponding occupation probabilities are small, so that these upper levels are effectively merged into the continuum. The absorption peak at $\log_{10} \hbar\omega/\text{eV} \approx 1.84$ in the left panel corresponds to the transition from the ground state to the state with $s = 1$ for the centered atoms. It would be a narrow spectral line without atomic motion. In the middle panel ($\alpha = -1$), there would be no significant bound-bound absorption at all, were the motion neglected. However, the thermal motion of atoms across the field drastically modifies the spectrum. There appears significant absorption for $\alpha = -1$. The bump at $\hbar\omega \approx 100$ eV for $\alpha = +1$ is due to the transition to the second excited level ($s = 2$), which would be negligible for nonmoving atoms. The magnetic broadening mentioned in § 4.2 smears the photoionization edges at $\hbar\omega \gtrsim 100$ eV and extends the bound-bound absorption frequency range down to ~ 10 eV for any polarization. The spikes near this low ω are explained by the $K_\perp$ dependence of the transition energy (Pavlov & Potekhin 1995). The spike at $\omega \approx \omega_{\text{cp}}$ ($\log_{10} \hbar\omega/\text{eV} \approx 1.17$) appears because the transitions between the decentered states whose quantum numbers s differ by one ($\Delta s = 1$) correspond to the energies $\approx \hbar\omega_{\text{cp}}$, almost independent of $K_\perp$ [it follows from eq. (14), since $E_{s\nu}^\parallel(K_\perp)$ is small at large $K_\perp$]. Another resonance occurs at a frequency slightly below ω_{cp}, which corresponds to the minimum distance between the states with $\Delta s = 1$ (the avoided crossings; cf. Potekhin 1994), because the energy difference

nonorthogonal ("collapse") at certain angles, so that their designation is ambiguous (Soffel et al. 1983).

The dotted curves in Figure 7 are obtained using equation (45). We see that this traditional calculation strongly overestimates κ_1 at large θ_B, and overestimates both κ_1 and κ_2 at $\theta_B = 0$, if $\hbar\omega$ is small enough.

Figure 8 shows the effective opacities κ^{eff} for the diffusion of nonpolarized radiation along ($\parallel$) and across ($\perp$) the magnetic field (§ 2.3), for the same plasma parameters as in Figure 7. The peak at $\log \hbar\omega/\text{eV} = 3.5$ is due to the ion cyclotron resonance, and the one at $\log \hbar\omega/\text{eV} = 3.9$ is due to the vacuum resonance. The barely visible intermediate spike at $\log \hbar\omega/\text{eV} = 3.8$ is the quantum resonance of the Coulomb logarithm at the doubled proton-cyclotron frequency (cf. Fig. 6).

We see that the improvement of the free-free cross section discussed in § 4.3.3 is important for the effective opacities shown in Figure 8 at $\omega < \omega_{\text{cp}}$. At $\omega \lesssim 0.3\omega_{\text{cp}}$, the difference exceeds 1 order of magnitude. Moreover, it has an impact on the Rosseland mean opacities, as discussed below.
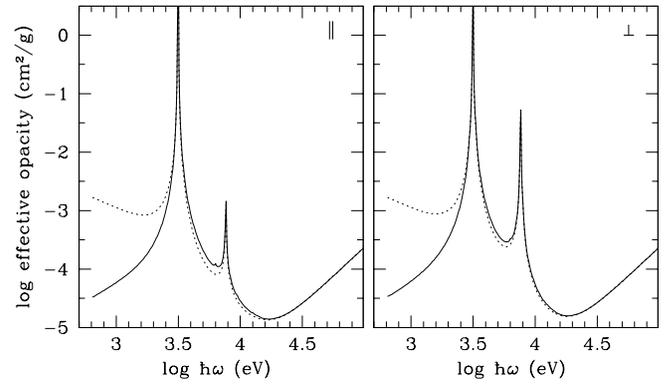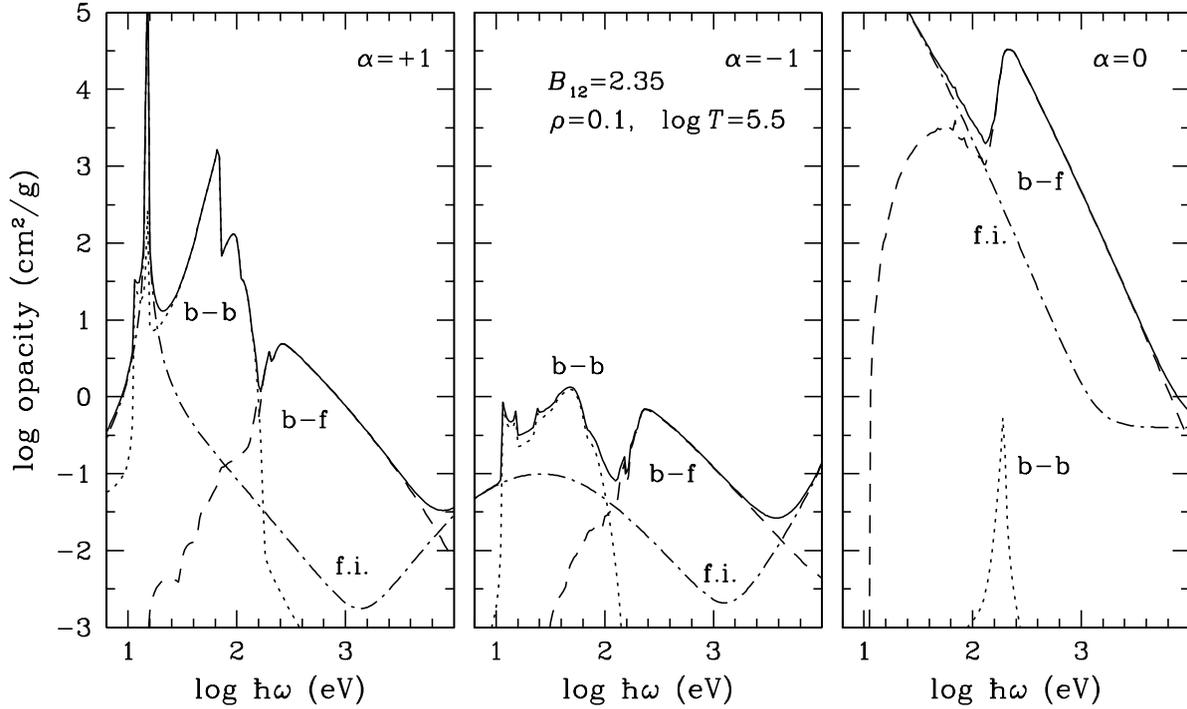
Fig. 9.—Monochromatic opacities for the basic polarizations ($\alpha = +1$, *left panel*; $\alpha = -1$, *middle panel*; $\alpha = 0$, *right panel*) in a typical partially ionized neutron star atmosphere at $\rho = 0.1$ g cm^{-3}, $T = 10^{5.5}$ K, and $B = 2.35 \times 10^{12}$ G. *Dot-dashed lines*: opacities of fully ionized component; *dashed lines*: bound-free opacities; *dotted lines*: bound-bound opacities; *solid lines*: total opacities.

has zero derivative with respect to K there. These resonances are smoothed by the electron impact broadening.

In general, we see that partial ionization must be taken into account in the opacity calculations at these plasma parameters.

Figure 10 shows the total extinction coefficients $\rho \kappa_\alpha$ for different ρ and T at $B = 10^{13}$ G. The curves are truncated from the left at $\omega = \omega_{pl}$. At $\rho = 50$ g cm^{-3}, the opacities are smooth functions of ω, which reflects the fact that virtually all excited atomic levels are merged into a continuum at these ρ and B. At $\rho \leq 2$ g cm^{-3}, however, the curves clearly reveal the features due to the bound-bound and bound-free transitions.

The opacities for the three basic polarizations, combined with appropriate components of the polarization vectors, provide the opacities in the two normal modes (§ 2.3). For example, Figure 11 shows the normal-mode opacities for $\rho = 0.1$ g cm^{-3} and $B = 10^{13}$ G, at three values of θ_B and two values of T. At the lower $T = 5 \times 10^5$ K, the features arising from the bound-bound and bound-free transitions are clearly visible at any θ_B.

5.3. *Rosseland Mean Opacities*

Along with the thermodynamic functions and number fractions of species, our tables contain Rosseland mean effective opacities for longitudinal ($\kappa_R^\parallel$) or transverse ($\kappa_R^\perp$) propagation of nonpolarized radiation. They are calculated in a standard way (e.g., Armstrong & Nicholls 1972) from the effective monochromatic opacities for the diffusion approximation, $\kappa^\parallel$ and $\kappa^\perp$, defined in § 2.3.

The improvement of the free-free cross section substantially affects $\kappa_R^\parallel$ and $\kappa_R^\perp$. For example, in the case of fully ionized plasma shown in Figure 8, we obtain $\kappa_R^\parallel = 1.8 \times 10^{-4}$

cm^2 g^{-1} and $\kappa_R^\perp = 1.6 \times 10^{-4}$ cm^2 g^{-1}, in reasonable agreement with the analytic fit in Potekhin & Yakovlev (2001) (2.1×10^{-4} and 1.7×10^{-4} cm^2 g^{-1}, respectively). Since the latter fit did not take into account the ion cyclotron resonance, we conclude that this resonance is unimportant for the Rosseland opacities in the given example. Meanwhile, the traditional treatment of this resonance (eq. [45]) yields effective opacities shown by the dotted lines in Figure 8, whose Rosseland means are $\kappa_R^\parallel = 1.3 \times 10^{-3}$ cm^2 g^{-1} and $\kappa_R^\perp = 1.0 \times 10^{-3}$ cm^2 g^{-1}, that is, about 6 times larger than the accurate values.

Figure 12 illustrates the density dependence of the Rosseland opacities at two values of T for $B = 10^{12}$ G and 2×10^{13} G. For comparison, the nonmagnetic OPAL opacities (Iglesias & Rogers 1996) are shown.[3] Dotted lines represent the effective Rosseland opacities in the model of a fully ionized electron-proton plasma, according to the fit of Potekhin & Yakovlev (2001).

As is well known, the strong magnetic field makes the atmosphere more transparent at given ρ and T, because of the presence of large ω_{ce} in the denominators of equations (33) and (49). At sufficiently large ρ, there is good agreement between the opacity tables and the analytic fully ionized plasma model. However, at $\rho \lesssim 1$–10 g cm^{-3}, there are large differences, which reflect the contribution of bound-bound and/or bound-free transitions in the effective opacities. Remarkably, this difference is significant at $T = 10^{5.5}$ K even in the nonmagnetic case (the upper curve in the left panel). As noted in Paper I, the contribution of bound species increases with increasing B.

---

[3] See http://www-phys.llnl.gov/Research/OPAL/. As mentioned in § 2D of Paper I, our model of partially ionized hydrogen plasma at $B = 0$ accurately reproduces the OPAL opacities.
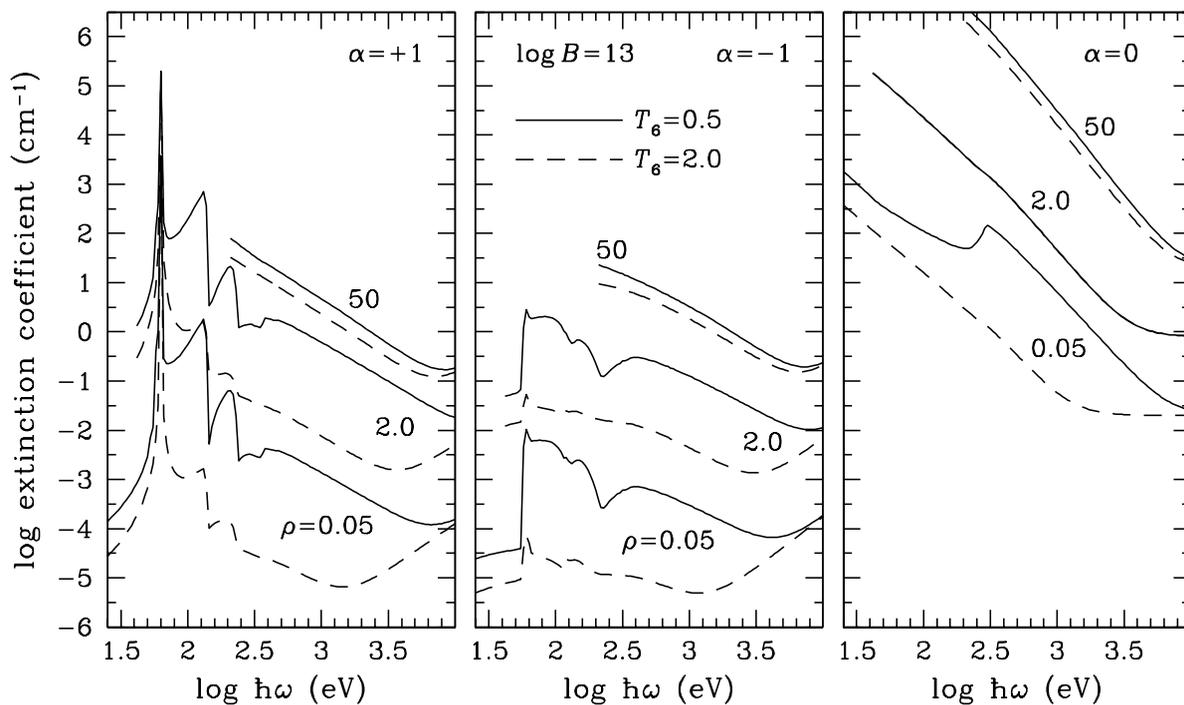
Fig. 10.—Monochromatic opacities for the same basic polarizations as in Fig. 9 at $T = 5 \times 10^5$ K (*solid lines*) and 2×10^6 K (*dashed lines*), $\rho = 0.05$, 2, and 50 g cm^{-3}, and $B = 10^{13}$ G.

In the case of $T = 10^{6.5}$ K (Fig. 12, *right panel*), the model of fully ionized plasma is quite accurate at $B \leq 10^{12}$ G. However, this is not the case at the higher field strength $B = 2 \times 10^{13}$ G, where the contribution from bound species is again appreciable.

6. DESCRIPTION OF THE TABLES

The input parameters for our tables are B, T, and the astrophysical density parameter $R = \rho_0 / T_6^3$. At present, the tables are calculated for $11.9 \leq \log_{10} B/\mathrm{G} \leq 13.5$
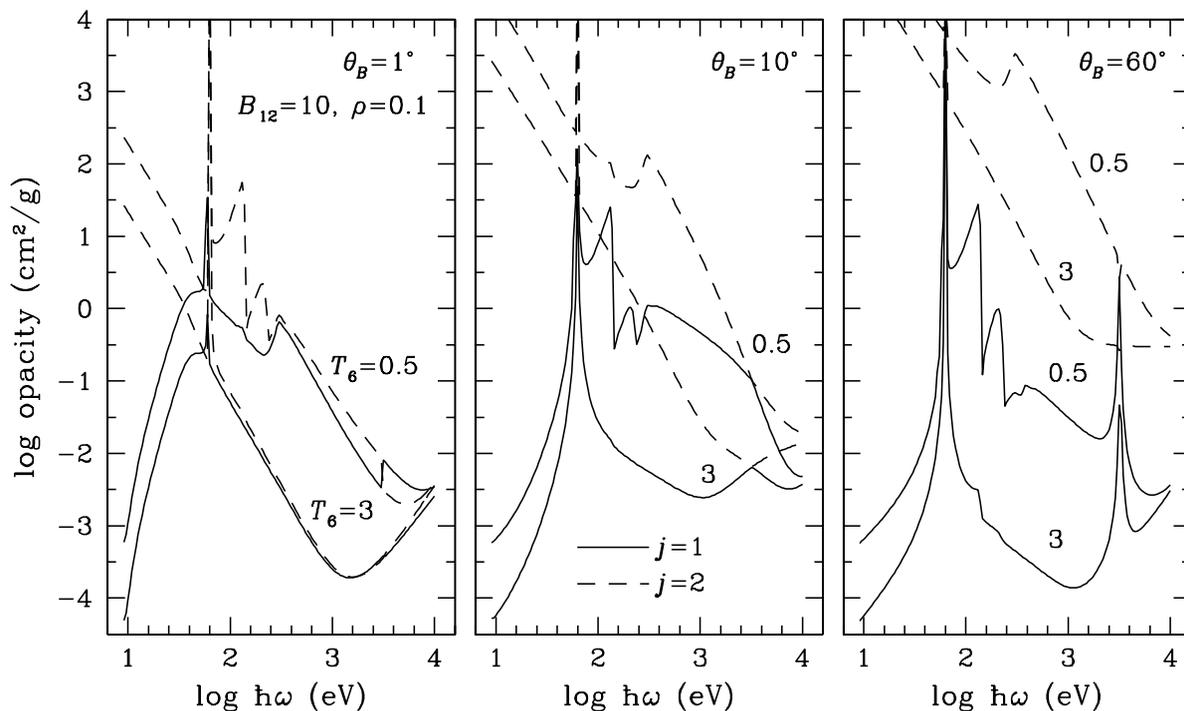

Fig. 11.—Monochromatic opacities for the extraordinary ($j = 1$, *solid lines*) and ordinary ($j = 2$, *dashed lines*) modes at $T = 5 \times 10^5$ K (*upper curves*) and 3×10^6 K (*lower curves*), for $\rho = 0.1$ g cm^{-3}, $B = 10^{13}$ G, and $\theta_B = 1°$, $10°$, and $60°$.
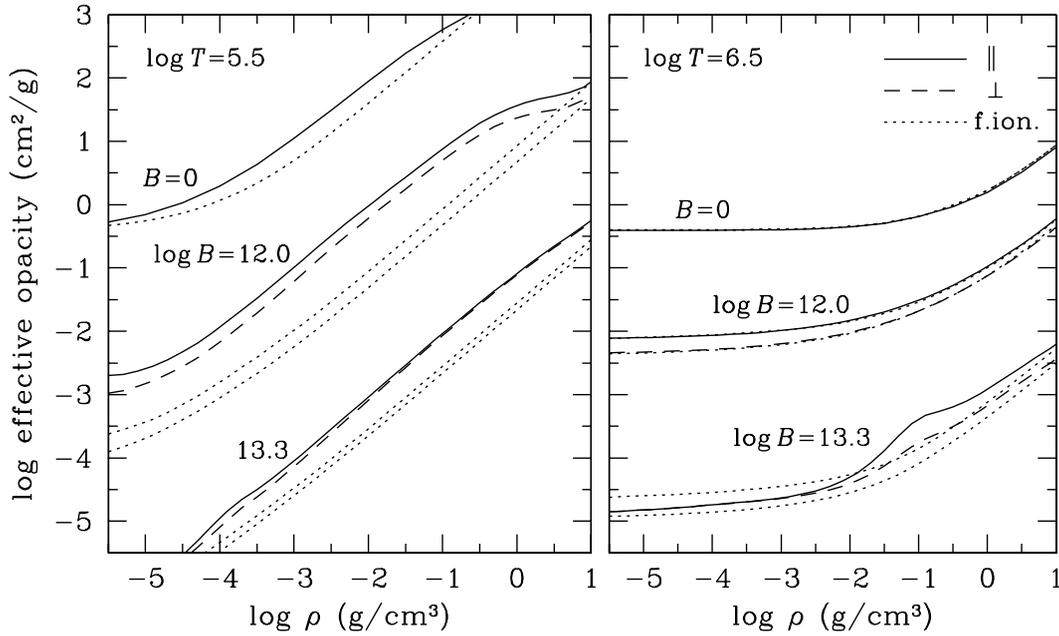
Fig. 12.—Effective Rosseland mean opacities for diffusion of nonpolarized radiation along (*solid lines*) or across (*dashed lines*) the magnetic field, at $T = 10^{5.5}$ K (*left panel*) and $10^{6.5}$ K, for $B = 0$, 10^{12}, and 2×10^{13} G. Dotted lines show the opacities of a fully ionized plasma (at each value of $B \neq 0$, the lower dotted curve corresponds to the transverse diffusion and the upper to the longitudinal one).

with step $\Delta \log_{10} B = 0.1$, $5.3 \leq \log_{10} T/\mathrm{K} \leq 7.0$ with step $\Delta \log_{10} T = 0.05$, and $-7.4 \leq \log_{10} R \leq 3.6$ with step $\Delta \log_{10} R = 0.2$.

The tables for different values of T and B have identical structure. An example is shown in Table 1. The first line contains $\log_{10} T/\mathrm{K}$ and $\log_{10} B/\mathrm{G}$. Each row then provides

1. $\log_{10} R$;
2. $\log_{10} P$, where $P = 10^6$ dyn cm^{-2} is the pressure in bars;
3. the dimensionless pressure parameter $PV/(N_0 k_B T)$, where N_0 is the total number of protons (free and bound) in volume V;
4. the dimensionless internal energy parameter $U/(N_0 k_B T)$;

5. the dimensionless entropy parameter $S/(N_0 k_B)$;
6. the reduced heat capacity $C_V/(N_0 k_B)$;
7. the logarithmic pressure derivative $\chi_T = (\partial \ln P/\partial \ln T)_V$;
8. the logarithmic pressure derivative $\chi_\rho = (\partial \ln P/\partial \ln \rho)_T$;
9. the atomic fraction x_H, that is, the total number of H atoms with nondissolved energy levels, divided by N_0;
10. the ground-state atomic fraction;
11. the molecular fraction (the number of H_2 molecules with nondestroyed levels, divided by N_0);
12. the fraction of protons comprised in clusters and in strongly perturbed atoms and molecules;
13. $\log_{10} \kappa^{\parallel}$, where $\kappa^{\parallel}$ is the effective Rosseland mean opacity for transport of nonpolarized radiation along

TABLE 1
SAMPLE EOS AND OPACITY TABLE

R	THERMODYNAMIC FUNCTIONS							NUMBER FRACTIONS				log (opacities)	
(1)	(2)	(3)	(4)	(5)	(6)	(7)	(8)	(9)	(10)	(11)	(12)	(13)	(14)
−7.40	0.8173	1.999	1.256	59.737	2.378	1.001	1.000	3.77E−04	7.15E−05	0.00E+00	7.81E−03	−4.896	−4.896
−7.20	1.0173	1.999	1.256	58.818	2.378	1.001	1.000	4.15E−04	8.30E−05	0.00E+00	8.85E−03	−4.872	−4.872
−0.20	7.9984	1.914	1.028	26.662	2.473	1.062	0.984	1.19E−02	8.10E−03	6.31E−11	9.91E−02	−1.242	−1.447
0.00	8.1949	1.898	0.977	25.736	2.501	1.074	0.980	1.33E−02	9.09E−03	1.77E−10	1.06E−01	−1.091	−1.295
0.20	8.3905	1.879	0.915	24.807	2.536	1.088	0.976	1.45E−02	1.01E−02	4.26E−10	1.13E−01	−0.954	−1.158
0.40	8.5853	1.857	0.841	23.873	2.575	1.105	0.971	1.51E−02	1.08E−02	8.15E−10	1.21E−01	−0.835	−1.039
0.60	8.7793	1.831	0.755	22.935	2.616	1.123	0.966	1.45E−02	1.09E−02	1.09E−09	1.32E−01	−0.738	−0.941
0.80	8.9721	1.801	0.654	22.000	2.658	1.142	0.963	1.23E−02	9.97E−03	8.36E−10	1.44E−01	−0.662	−0.866
3.00	10.9665	1.122	−1.917	11.401	2.765	1.935	0.692	0.00E+00	0.00E+00	0.00E+00	1.50E−02	2.207	2.039
3.20	11.1018	0.967	−2.457	10.364	2.836	2.276	0.670	0.00E+00	0.00E+00	0.00E+00	3.76E−03	3.083	2.904
3.40	11.2407	0.840	−3.068	9.334	2.900	2.651	0.734	0.00E+00	0.00E+00	0.00E+00	4.11E−04	4.248	4.055
3.60	11.4056	0.775	−3.736	8.301	2.946	2.906	0.975	0.00E+00	0.00E+00	0.00E+00	1.40E−05	5.782	5.574

magnetic field lines in the diffusion approximation, in cm^2 g^{-1}; and

14. $\log_{10} \kappa^\perp$, where $\kappa^\perp$ is analogous to $\kappa^\parallel$, but for diffusion of radiation in the direction perpendicular to $\boldsymbol{B}$.

We have also written a Fortran program for the cubic polynomial interpolation of the tabulated data in the three-parameter space of B, T, and ρ.[4]

7. CONCLUSIONS

We have calculated the EOS and radiative opacities of fully and partially ionized hydrogen plasmas in a wide range of densities, temperatures, and magnetic fields typical for photospheres of the strongly magnetized neutron stars. The first- and second-order thermodynamic functions, nonionized fractions, and effective Rosseland mean opacities are published in electronic form.[5]

The opacities are calculated more accurately than in the previous publications. In particular, we take into account suppression of the free-free absorption below the proton cyclotron frequency, which was overlooked previously. This effect reduces the opacities of the ionized component of the plasma by orders of magnitude at photon energies $\hbar\omega \lesssim 0.3\hbar\omega_{\rm cp} \sim 0.02B_{12}$ keV, which necessitates a revision of the previously published models of X-ray spectra of magnetars (Zane et al. 2001; Ho & Lai 2001, 2003; Özel 2001, 2003). On the other hand, the bound-bound and bound-free absorption, neglected in the previous models of neutron star atmospheres, increases the opacities by more than 1 order of magnitude at $\hbar\omega \sim 0.1$–3 keV in the outer atmosphere layers of the ordinary neutron stars with $B \sim 10^{12}$–$10^{13.5}$ G and $T < (1$–$3) \times 10^6$ K, which can also significantly affect the spectra.

One can expect that the effect of the bound species on the EOS and opacities is as important for magnetars (despite their supposedly higher temperatures) as for the ordinary neutron stars. To check this, we need to extend our model to higher B; preliminary high-B results (Chabrier et al. 2002) support this anticipation.

---

[4] The tables and the program are available at http://www.ioffe.rssi.ru/astro/NSG/Hmagnet/.
[5] See footnote 4.

APPENDIX A

PHOTOABSORPTION DUE TO PROTON-PROTON COLLISIONS

The general formula for the differential cross section of absorption of radiation by a quantum mechanical system is (e.g., Armstrong & Nicholls 1972)

$$d\sigma = \frac{4\pi^2}{\omega c} |\boldsymbol{e} \cdot \langle f|\boldsymbol{j}_{\rm eff}|i\rangle|^2 \delta(E_f - E_i - \hbar\omega) d\nu_f \, , \tag{A1}$$

where i and f are the initial and final states of the system, $d\nu_f$ is the density of final states, $\boldsymbol{e}$ is the polarization vector, $\boldsymbol{j}_{\rm eff} = e^{i\boldsymbol{k}_\gamma \cdot \boldsymbol{r}}\boldsymbol{j}$, $\boldsymbol{j}$ is the electric current operator, and $\boldsymbol{k}_\gamma$ is the photon wavenumber. For two charged particles in a magnetic field,

$$\boldsymbol{j}_{\rm eff} = \left(\frac{e^{i\boldsymbol{k}_\gamma \cdot \boldsymbol{r}_1} q_1 \boldsymbol{\pi}_1}{m_1} + \frac{e^{i\boldsymbol{k}_\gamma \cdot \boldsymbol{r}_2} q_2 \boldsymbol{\pi}_2}{m_2} \right) \, , \tag{A2}$$

where q_i and m_i are the particle charge and mass ($i = 1, 2$), and $\boldsymbol{\pi}_i$ is given by equation (3). Introducing, in the standard way, the center-of-mass ($\boldsymbol{R}$, $\boldsymbol{P}$) and relative ($\boldsymbol{r}$, $\boldsymbol{p}$) coordinates and momenta of two protons and using the gauge $\boldsymbol{A}(\boldsymbol{r}_i) = \frac{1}{2}\boldsymbol{B} \times \boldsymbol{r}_i$, we get

$$\boldsymbol{j}_{\rm eff} = e^{i\boldsymbol{k}_\gamma \cdot \boldsymbol{R}} \frac{e}{m_p} \left[\boldsymbol{P} - \frac{e}{c}\boldsymbol{B} \times \boldsymbol{R} + i(\boldsymbol{k}_\gamma \cdot \boldsymbol{r})\left(\boldsymbol{p} - \frac{e}{4c}\boldsymbol{B} \times \boldsymbol{r}\right) \right] + O(\boldsymbol{k}_\gamma \cdot \boldsymbol{r})^2 \, . \tag{A3}$$

The first two terms do not contribute to the free-free absorption, because they do not contain the relative variables and, therefore, are decoupled from the Coulomb interaction. The remaining terms are similar to $\boldsymbol{j}_{\rm eff}$ relevant to absorption of radiation by a particle with charge $e/2$ and mass m_p, except for the factor $\boldsymbol{k}_\gamma \cdot \boldsymbol{r}$, which is small at $\hbar\omega \ll m_p c^2$. The absorption cross section can be written in the form of equation (46). The nonquantizing magnetic field, $\beta_p \ll 1$, does not affect the effective collision frequency ν_α^{pp}, which in this case does not depend on α. We have evaluated the proton free-free cross section in the nonrelativistic Born approximation, using the technique of Fourier transforms (Bethe & Salpeter 1957, § 77). For two distinguishable particles of equal mass m_p and charge e, the cross section is

$$\sigma_*^{pp}(p_i, \omega) = \frac{256\pi^2}{3} \frac{n_p e^6}{m_p c \hbar\omega^3} \frac{1}{p_i} \left[\frac{p_i p_f}{(m_p c)^2} + \frac{3}{10} \frac{p_i^2 + p_f^2}{(m_p c)^2} \ln\left|\frac{p_f + p_i}{p_f - p_i}\right| \right] \, . \tag{A4}$$

Taking into account that the colliding protons are identical and have spin $\frac{1}{2}$, one should calculate the matrix element in

equation (A1) for symmetric and antisymmetric final states and sum up the cross sections with the statistical weights $\frac{1}{4}$ and $\frac{3}{4}$, respectively (e.g., Landau & Lifshitz 1976). This leads to the equation

$$\sigma^{pp}(p_i, \omega) = 2\sigma^{pp}_*(p_i, \omega) - \sigma^{pp}_\times(p_i, \omega) , \tag{A5}$$

where

$$\sigma^{pp}_\times(p_i, \omega) = \frac{128\pi^2}{3} \frac{n_p e^6}{m_p c \hbar \omega^3} \frac{1}{p_i} \left[\frac{6}{5} \frac{p_i p_f}{(m_p c)^2} \frac{p_i^4 + p_f^4}{(p_i^2 + p_f^2)^2} + \left(\frac{\hbar\omega}{c}\right)^2 \frac{p_i^4 + p_f^4 + 0.8 p_i^2 p_f^2}{(p_i^2 + p_f^2)^3} \ln\left|\frac{p_f + p_i}{p_f - p_i}\right| \right] . \tag{A6}$$

In equations (A4) and (A6), $p_f^2 = p_i^2 + m_p \hbar \omega$, since the reduced mass equals $m_p/2$. The Maxwell distribution for the relative momenta is $\mathscr{F}_{pp}(p_i) = (4/\pi^{1/2})(m_p k_B T)^{-3/2} p_i^2 \exp(-p_i^2/m_p k_B T)$. Averaging of equation (A5) with this distribution gives the cross section in the form (45) with ν^{pp} given by equation (47), where Λ_{pp} is calculated by averaging the p_i-dependent factors of equations (A4) and (A6).

APPENDIX B

PHOTOABSORPTION DUE TO ELECTRON-PROTON COLLISIONS

In the case of photoabsorption due to the electron-proton collisions, the initial and final states in equation (A1) are the continuum states of the hydrogen atom described by equation (6). The wave function of the relative electron-proton motion can be written as

$$\psi(\mathbf{r}) = \psi_0(\mathbf{r}) + \psi_1(\mathbf{r}), \qquad \psi_0(\mathbf{r}) = \frac{e^{ik_0 z}}{\sqrt{L}} \Phi_{ns}(\mathbf{r}_\perp) , \tag{B1}$$

where $\psi_0(\mathbf{r})$ describes free motion with z-component of the relative momentum $\hbar k_0$, L is the normalization length, and $\psi_1(\mathbf{r})$ is a perturbation due to the Coulomb interaction. Let us apply one-dimensional Fourier transformation:

$$\tilde{\psi}(\mathbf{r}_\perp, k) = \frac{1}{\sqrt{L}} \int_{-L/2}^{L/2} e^{-ikz} \psi(\mathbf{r}) dz . \tag{B2}$$

In the limit of $L \to \infty$, we will have $\tilde{\psi}_0(\mathbf{r}_\perp, k) \to (2\pi/L)\delta(k - k_0)\Phi_{ns}(\mathbf{r}_\perp)$. Let us use expansion (11) for $\psi_1(\mathbf{r})$; then

$$\tilde{\psi}_1(\mathbf{r}_\perp, k) = \sum_{n's'} \tilde{g}_{n's'}(k)\Phi_{ns}(\mathbf{r}_\perp) . \tag{B3}$$

This is equivalent to replacing $g_{n's'}(z)$ by $L^{-1/2} \exp(ik_0 z)\delta_{nn'}\delta_{ss'} + g_{n's'}(z)$ in equations (12) and (15). Then, applying the Fourier transformation to equation (15) with $\mathbf{r}_0 = \mathbf{r}_c$ and treating ψ_1 as small perturbation, in the first approximation we obtain

$$\left[\left(\frac{\hbar^2}{2\mu}\right) (k^2 - k_0^2) + E_{n's'}^\perp - E_{ns}^\perp \right] \tilde{g}_{n's'}(k) = -L^{-1} \tilde{V}_{ns,n's'}(\mathbf{r}_c, k - k_0) , \tag{B4}$$

where

$$\tilde{V}_{ns,n's'}(\mathbf{r}_c, k) = \int_{-\infty}^{\infty} e^{-ikz} V_{ns,n's'}(\mathbf{r}_c, z) dz . \tag{B5}$$

Using equations (A3)–(A10) of Potekhin (1994), we can convert $\tilde{V}_{ns,n's'}(\mathbf{r}_c, k)$ into

$$\tilde{V}_{ns,n's'}(\mathbf{r}_c, k) = -e^2 \tilde{v}_{ns,n's'}\left(\frac{a_m K_\perp}{\sqrt{2}}, \sqrt{2}a_m k\right) , \tag{B6}$$

where

$$\tilde{v}_{ns,n's'}(\rho, \kappa) = (-1)^{(|s|-s+|s'|-s')/2} \sum_{l=0}^{n_\rho + n'_\rho} (-1)^l \sum_{m=\max(0,l-n'_\rho)}^{\min(n_\rho,l)} a_{mn_\rho|s|} a_{l-m,n'_\rho,|s'|} \sqrt{\tilde{s}\tilde{s}'} \tilde{v}_{0\tilde{s},0\tilde{s}'}(\rho, \kappa) , \tag{B7}$$

and, assuming $q \geq 0$,

$$\tilde{v}_{0,s,0,s+q}(\rho, \kappa) = \tilde{v}_{0,s+q,0,s}(\rho, \kappa) = \rho^q \sum_{m=0}^{s} a_{msq} \rho^{2m} \int_0^1 \exp\left(-\frac{\kappa^2}{4}\frac{1-t}{t} - \rho^2 t\right) t^{2m+q-1} (1-t)^{s-m} dt . \tag{B8}$$

In equations (B7) and (B8), we have defined

$$n_\rho = n + \frac{s - |s|}{2}, \quad n'_\rho = n' + \frac{s' - |s'|}{2}, \tag{B9a}$$

$$\tilde{s} = \frac{|s| + s + |s'| - s'}{2} + l, \qquad \tilde{s}' = \frac{|s| - s + |s'| + s'}{2} + l, \tag{B9b}$$

$$a_{mns} = \frac{\sqrt{n!(n + s)!}}{m!(n - m)!(m + s)!} \tag{B9c}$$

(n_ρ and n'_ρ are the radial quantum numbers of the Landau functions; e.g., Landau & Lifshitz 1976).

For fixed quantum numbers n_f, s_f, and a fixed sign of the z-projection of the relative momentum k_f of the final state, $d\nu_f$ in equation (A1) equals $L\,dk_f/2\pi = (L/2\pi)(\mu/\hbar^2|k_f|)dE_f$. Therefore, the cross section of photoabsorption by an electron-proton pair with initial quantum numbers n_i and s_i, longitudinal wavevector k_i, and transverse pseudomomentum $K_\perp$ is

$$\sigma(k_i, K_\perp, n_i, s_i, \omega) = \sum_{n_f, s_f, \text{sign}k_f} \frac{2\pi L\mu}{\hbar^2|k_f|\omega c}|\boldsymbol{e} \cdot \langle f|\boldsymbol{j}_{\text{eff}}|i\rangle|^2. \tag{B10}$$

Here, the sum is performed over those n_f and s_f that are permitted by the energy conservation law,

$$E_{n_f s_f}^\perp + \frac{\hbar^2 k_f^2}{2\mu} = E_{n_i s_i}^\perp + \frac{\hbar^2 k_i^2}{2\mu} + \hbar\omega. \tag{B11}$$

A general expression for $\boldsymbol{j}_{\text{eff}}$ has been derived by Potekhin & Pavlov (1997). In the dipole approximation, it reduces to

$$\boldsymbol{j}_{\text{eff}} = e\left(\frac{\boldsymbol{\pi}}{m_e} + \frac{\boldsymbol{\Pi}}{m_p}\right), \tag{B12}$$

where $\boldsymbol{\pi}$ is defined by equation (9) and

$$\boldsymbol{\Pi} = \boldsymbol{p} - \frac{e}{2c}\boldsymbol{B} \times \boldsymbol{r}. \tag{B13}$$

The circular components of operators $\boldsymbol{\pi}$ and $\boldsymbol{\Pi}$, $\pi_{\pm 1} = (\pi_x \pm i\pi_y)/\sqrt{2}$ and $\Pi_{\pm 1} = (\Pi_x \pm i\Pi_y)/\sqrt{2}$, transform one Landau state $|n, s\rangle_\perp$, characterized by the function $\Phi_{ns}(\boldsymbol{r}_\perp)$, into another Landau state,[6]

$$\pi_{+1}|n, s\rangle_\perp = -\frac{i\hbar}{a_m}\sqrt{n+1}|n+1, s-1\rangle_\perp, \tag{B14a}$$

$$\pi_{-1}|n, s\rangle_\perp = \frac{i\hbar}{a_m}\sqrt{n}|n-1, s+1\rangle_\perp, \tag{B14b}$$

$$\Pi_{+1}|n, s\rangle_\perp = -\frac{i\hbar}{a_m}\sqrt{n+s}|n, s-1\rangle_\perp, \tag{B14c}$$

$$\Pi_{-1}|n, s\rangle_\perp = \frac{i\hbar}{a_m}\sqrt{n+s+1}|n, s+1\rangle_\perp. \tag{B14d}$$

Since $\boldsymbol{e} \cdot \boldsymbol{j} = e_{+1}j_{-1} + e_0 j_0 + e_{-1}j_{+1}$, the matrix element with π_{+1} and Π_{+1} contributes to σ_{-1}, and vice versa.

In the first Born approximation, using equations (B4), (B11), (B12), and (B14), we obtain

$$\langle f|\boldsymbol{j}_{\text{eff}}|i\rangle_0 = \frac{e}{L\mu\omega}(k_i - k_f)\tilde{V}_{n_i s_i n_f s_f}, \tag{B15a}$$

$$\langle f|\boldsymbol{j}_{\text{eff}}|i\rangle_{-1} = -\frac{ie}{La_m}\left[\frac{\sqrt{n_f + 1}\,\tilde{V}_{n_i s_i, n_f+1, s_f-1} - \sqrt{n_i}\,\tilde{V}_{n_i-1, s_i+1, n_f s_f}}{m_e(\omega + \omega_{\text{ce}})}\right.$$
$$\left. \times \frac{\sqrt{n_f + s_f}\,\tilde{V}_{n_i s_i, n_f, s_f-1} - \sqrt{n_i + s_i + 1}\,\tilde{V}_{n_i, s_i+1, n_f s_f}}{m_p(\omega - \omega_{\text{cp}})}\right], \tag{B15b}$$

$$\langle f|\boldsymbol{j}_{\text{eff}}|i\rangle_{+1} = \frac{ie}{La_m}\left[\frac{\sqrt{n_f}\,\tilde{V}_{n_i s_i, n_f-1, s_f+1} - \sqrt{n_i + 1}\,\tilde{V}_{n_i+1, s_i-1, n_f s_f}}{m_e(\omega - \omega_{\text{ce}})}\right.$$
$$\left. \times \frac{\sqrt{n_f + s_f + 1}\,\tilde{V}_{n_i s_i, n_f, s_f+1} - \sqrt{n_i + s_i}\,\tilde{V}_{n_i, s_i-1, n_f s_f}}{m_p(\omega + \omega_{\text{cp}})}\right]. \tag{B15c}$$

Here, for brevity, $\tilde{V}_{nsn's'} \equiv \tilde{V}_{nsn's'}(r_c, k_f - k_i)$.

---

[6] The square root factors in eqs. (B14c) and (B14d) were interchanged by mistake in the corresponding eq. (A3b) of Potekhin & Pavlov (1997).

Equations (B10) and (B15) provide the partial cross sections for one electron-proton pair in a given state. Provided there are n_e electrons per unit volume, the number of electrons interacting with a given proton and having k_i in the interval dk_i and r_c in the surface element $d^2 r_c$ is

$$dn_i = n_e L \, d^2 r_c \mathscr{F}_{\parallel}(k_i) dk_i \mathscr{F}_{n_i s_i} \, . \tag{B16}$$

Here

$$\mathscr{F}_{\parallel}(k_i) = \hbar (2\pi \mu k_{\mathrm B} T)^{-1/2} \exp\left(\frac{-\hbar^2 k_i^2}{2\mu k_{\mathrm B} T}\right) \tag{B17}$$

is the Maxwell distribution of the continuum states over k_i, and

$$\mathscr{F}_{n_i s_i} = \left(1 - e^{-\beta_e}\right)\left(1 - e^{-\beta_p}\right) \exp\left[-n_i \beta_e - (n_i + s_i)\beta_p\right] \tag{B18}$$

is the Boltzmann distribution over $n_i \geq 0$ and $s_i \geq -n_i$. Thus the total cross section is

$$\sigma(\omega, T, B) = n_e L \pi a_m^4 \sum_{n_i s_i} \mathscr{F}_{n_i s_i} \int_{-\infty}^{\infty} \mathscr{F}_{\parallel}(k_i) dk_i \int_0^{\infty} K_\perp \, dK_\perp \sigma(k_i, K_\perp, n_i, s_i, \omega) \, . \tag{B19}$$

For every polarization, let us write $\sigma(\omega, T, B)$ in the form of equation (49). Then

$$\Lambda_\alpha^e = \frac{3}{4} \sum_{n_i s_i} \mathscr{F}_{n_i s_i} \sum_{n_f, s_f, \mathrm{sign}\kappa_f} \int_0^{\infty} \frac{d\kappa_i}{|\kappa_f|} \exp\left[-\left(\beta_e + \beta_p\right)\frac{\kappa_i^2}{4}\right] w_{n_i s_i n_f s_f}^{\alpha}(\kappa_f - \kappa_i) \, , \tag{B20}$$

where, taking into account equation (B11), we have

$$\kappa_f^2 = \kappa_i^2 + 4(n_i - n_f) + 4\frac{m_e}{m_{\mathrm H}}(s_i - s_f) + 4\frac{m_p}{m_{\mathrm H}}\frac{u}{\beta_e} \, , \tag{B21}$$

and the functions $w_{n_i s_i n_f s_f}^{\alpha}(\kappa_f - \kappa_i)$ in the integrand are defined according to equations (B6), (B15), and (B19) as

$$w_{nsn's'}^0(\kappa) = \kappa^2 \int_0^{\infty} \rho \, d\rho |\tilde{v}_{nsn's'}(\rho, \kappa)|^2 \, , \tag{B22a}$$

$$w_{nsn's'}^{-1}(\kappa) = \frac{2}{(1 + m_e/m_p)^2} \int_0^{\infty} \rho \, d\rho \Big| \sqrt{n'}\tilde{v}_{ns,n'-1,s'+1}(\rho, \kappa) - \sqrt{n+1}\tilde{v}_{n+1,s-1,n's'}(\rho, \kappa)$$
$$+ \frac{m_e}{m_p}\frac{\omega - \omega_{\mathrm{ce}}}{\omega + \omega_{\mathrm{cp}}}\left[\sqrt{n'+s'+1}\tilde{v}_{nsn',s'+1}(\rho, \kappa) - \sqrt{n+s}\tilde{v}_{n,s-1,n's'}(\rho, \kappa)\right]\Big|^2 \, , \tag{B22b}$$

$$w_{nsn's'}^{+1}(\kappa) = \frac{2}{(1 + m_e/m_p)^2} \int_0^{\infty} \rho \, d\rho \Big| \sqrt{n'+1}\tilde{v}_{ns,n'+1,s'-1}(\rho, \kappa) - \sqrt{n}\tilde{v}_{n-1,s+1,n's'}(\rho, \kappa)$$
$$+ \frac{m_e}{m_p}\frac{\omega + \omega_{\mathrm{ce}}}{\omega - \omega_{\mathrm{cp}}}\left[\sqrt{n'+s'}\tilde{v}_{nsn',s'-1}(\rho, \kappa) - \sqrt{n+s+1}\tilde{v}_{n,s+1,n's'}(\rho, \kappa)\right]\Big|^2 \, . \tag{B22c}$$

REFERENCES

Adler, S. L. 1971, Ann. Phys., 67, 599
Armstrong, B. M., & Nicholls, R. W. 1972, Emission, Absorption and Transfer of Radiation in Heated Atmospheres (Oxford: Pergamon)
Bethe, H. A., & Salpeter, E. E. 1957, Quantum Mechanics of One- and Two-Electron Atoms (Berlin: Springer)
Bezchastnov, V. G., & Potekhin, A. Y. 1994, J. Phys. B, 27, 3349
Blandford, R. D., & Hernquist, L. 1982, J. Phys. C, 15, 6233
Brown, E. F., Bildsten, L., & Chang, P. 2002, ApJ, 574, 920
Bulik, T., & Pavlov, G. G. 1996, ApJ, 469, 373
Canuto, V., & Ventura, J. 1977, Fundam. Cosmic Phys., 2, 203
Chabrier, G. 1990, J. Phys. (France), 51, 1607
Chabrier, G., Douchin, F., & Potekhin, A. Y. 2002, J. Phys. Condensed Matter, 14, 9133
Chabrier, G., & Potekhin, A. Y. 1998, Phys. Rev. E., 58, 4941
Chandrasekhar, S. 1961, Hydrodynamic and Hydromagnetic Stability (Oxford: Clarendon)
Däppen, W., Anderson, L., & Mihalas, D. 1987, ApJ, 319, 195
Forster, H., Strupat, W., Rösner, W., Wunner, G., Ruder, H., & Herold, H. 1984, J. Phys. B, 17, 1301
Ginzburg, V. L. 1970, The Propagation of Electromagnetic Waves in Plasmas (2d ed.; London: Pergamon)
Gnedin, Yu. N., & Pavlov, G. G. 1973, Zh. Eksper. Teor. Fiz., 65, 1806 (English transl., Soviet Phys.–JETP Lett., 38, 903 [1974])
Gor'kov, L. P., & Dzyaloshinskii, I. E. 1967, Zh. Eksper. Teor. Fiz., 53, 717 (English transl., Soviet Phys.–JETP Lett., 26, 449 [1968])

Heyl, J. S., & Hernquist, L. 1997a, J. Phys. A, 30, 6485
———. 1997b, Phys. Rev. D, 55, 2449
Ho, W. C. G., & Lai, D. 2001, MNRAS, 327, 1081
———. 2003, MNRAS, 338, 233
Hummer, D. G. 1988, ApJ, 327, 477
Iglesias, C. A., & Rogers, F. J. 1996, ApJ, 464, 943
Inglis, D. R., & Teller, E. 1939, ApJ, 90, 439
Kaminker, A. D., Pavlov, G. G., & Shibanov, Yu. A. 1982, Ap&SS, 86, 249
Karzas, W. J., & Latter, R. 1961, ApJS, 6, 167
Kopidakis, N., Ventura, J., & Herold, H. 1996, A&A, 308, 747
Lai, D. 2001, Rev. Mod. Phys., 73, 629
Lai, D., & Ho, W. C. G. 2002, ApJ, 566, 373
Lai, D., & Salpeter, E. E. 1995, Phys. Rev. A, 52, 2611
———. 1997, ApJ, 491, 270
Landau, L. D., & Lifshitz, E. M. 1976, Quantum Mechanics (Oxford: Pergamon)
———. 1993, Statistical Physics, Part 1 (Oxford: Pergamon)
Mereghetti, S. 2001, in The Neutron Star–Black Hole Connection, ed. C. Kouveliotou, J. Ventura, & E. P. J. van den Heuvel (NATO ASI Ser. C, 567; Dordrecht: Kluwer), 351
Mészáros, P. 1992, High-Energy Radiation from Magnetized Neutron Stars (Chicago: Univ. Chicago Press)
Miller, M. C. 1992, MNRAS, 255, 129
Miralles, J. A., Urpin, V., & van Riper, K. 1997, ApJ, 480, 358
Nagel, W. 1980, ApJ, 236, 904

Özel, F. 2001, ApJ, 563, 276
———. 2003, ApJ, 583, 402
Özel, F., Psaltis, D., & Kaspi, V.M. 2001, ApJ, 563, 255
Page, D., Shibanov, Yu. A., & Zavlin, V. E. 1995, ApJ, 451, L21
———. 1996, in MPE Rep. 263, Röntgenstrahlung from the Universe, ed.
    H. U. Zimmermann, J. E. Trümper, & H. Yorke (Garching: MPE), 173
Pavlov, G. G., & Gnedin, Yu. N. 1984, Astrophys. Space Phys. Rev., 3, 197
Pavlov, G. G., & Mészáros, P. 1993, ApJ, 416, 752
Pavlov, G. G., & Panov, A. N. 1976, Zh. Eksper. Teor. Fiz., 71, 572
    (English transl., Soviet Phys.–JETP Lett., 44, 300 [1976])
Pavlov, G. G., & Potekhin, A. Y. 1995, ApJ, 450, 883
Pavlov, G. G., Shibanov, Yu. A., Zavlin, V. E., & Meyer, R. D. 1995, in
    The Lives of the Neutron Stars, ed. M. A. Alpar, Ü. Kiziloğlu, & J. van
    Paradijs (NATO ASI Ser. C, 450; Dordrecht: Kluwer), 71
Potekhin, A. Y. 1994, J. Phys. B, 27, 1073
———. 1996a, A&A, 306, 999
———. 1996b, Phys. Plasmas, 3, 4156
———. 1998, J. Phys. B, 31, 49
Potekhin, A. Y., & Chabrier, G. 2000, Phys. Rev. E, 62, 8554
Potekhin, A. Y., Chabrier G., & Shibanov, Yu. A. 1999, Phys. Rev. E, 60,
    2193 (Paper I)
———. 2000, in ASP Conf. Ser. 202, Pulsar Astronomy—2000 and
    Beyond, ed. M. Kramer, N. Wex, & R. Wielebinski (IAU Colloq. 177;
    San Francisco: ASP), 619
Potekhin, A. Y., & Pavlov, G. G. 1993, ApJ, 407, 330
———. 1997, ApJ, 483, 414
Potekhin, A. Y., Pavlov, G. G., & Ventura, J. 1997, A&A, 317, 618
Potekhin, A. Y., & Yakovlev, D. G. 2001, A&A, 374, 213
Rajagopal, M., Romani, R., & Miller, M. C. 1997, ApJ, 479, 347

Saumon, D., & Chabrier, G. 1991, Phys. Rev. A, 44, 5122
———. 1992, Phys. Rev. A, 46, 2084
Saumon, D., Chabrier, G., & Van Horn, H. M. 1995, ApJS, 99, 713
Seaton, M. J., Yan, Y., Mihalas, D., & Pradhan, A. K. 1994, MNRAS,
    266, 805
Shafranov, V. D. 1967, in Reviews of Plasma Physics, vol. 3, ed.
    M. A. Leontovich (New York: Consultants Bureau), 1
Shibanov, Yu. A., Pavlov, G. G., Zavlin, V. E., & Ventura, J. 1992, A&A,
    266, 313
Shibanov, Yu. A., & Zavlin, V. E. 1995, Astron. Lett., 21, 3
Silant'ev, N. A., & Yakovlev, D. G. 1980, Ap&SS, 71, 45
Soffel, M., Ventura, J., Herold, H., Ruder, H., & Nagel, W. 1983, A&A,
    126, 251
Stehlé, C., & Jacquemot, S. 1993, A&A, 271, 348
Taylor, J. H., Manchester, R. N., & Lyne, A. G. 1993, ApJS, 88, 529
Thompson, C., Duncan, R. C., Woods, P. M., Kouveliotou, C.,
    Finger, M. H., & van Paradijs, J. 2000, ApJ, 543, 340
Ventura, J. 1979, Phys. Rev. D, 19, 1684
Ventura, J., & Potekhin, A. Y. 2001, in The Neutron Star–Black Hole
    Connection, ed. C. Kouveliotou, J. Ventura, & E. P. J. van den Heuvel
    (NATO ASI Ser. C, 567; Dordrecht: Kluwer), 393
Ventura, J., Soffel, M., Herold, H., & Ruder, H. 1985, A&A, 144, 479
Vincke, M., Le Dourneuf, M., & Baye, D. 1992, J. Phys. B, 25, 2787
Wigner, E. P., & Eisenbud, L. 1947, Phys. Rev., 72, 29
Zane, S., Turolla, R., Stella, L., & Trevis, A. 2001, ApJ, 560, 384
Zane, S., Turolla, R., & Trevis, A. 2000, ApJ, 537, 387
Zavlin, V. E., Pavlov, G. G., Shibanov, Yu. A., & Ventura, J. 1995, A&A,
    297, 441